Report Prepared by:

L. V. Taveira
A. A. Sagüés
J. Lopez-Sabando
B. Joseph

EARLY WARNING CORROSION DETECTION IN POST TENSIONED TENDONS

Contract No. BD544-08
Final Report to Florida Department of Transportation

Alberto A. Sagüés
Principal Investigator
Department of Civil and Environmental Engineering
Babu Joseph
Department of Chemical Engineering
Co-Principal Investigator
October 31, 2007

University of South Florida
Tampa, FL, 33620

1. Report No.	2. Government Accession No.	3. Recipient's Catalog No.

4. Title and Subtitle	5. Report Date
EARLY WARNING CORROSION DETECTION IN POST TENSIONED TENDONS	October 31, 2007
	6. Performing Organization Code
	8. Performing Organization Report No.
7. Author's	
L. V. Taveira, A. A. Sagüés, J. Lopez-Sabando, B. Joseph	

9. Performing Organization Name and Address	10. Work Unit No. (TRAIS)
Department of Civil and Environmental Engineering University of South Florida Tampa, FL 33620	11. Contract or Grant No. BD544-08
	13. Type of Report and Period Covered Final Report 10/06/03 - 10/31/07
12. Sponsoring Agency Name and Address	14. Sponsoring Agency Code
Florida Department of Transportation 605 Suwannee Street Tallahassee, FL 32399-0450	

15. Supplementary Notes

Prepared in cooperation with the U.S. Department of Transportation and the Federal Highway Administration.

16. Abstract

The feasibility and sensitivity of electrochemical noise (EN), electrochemical impedance spectroscopy (EIS), and linear polarization resistance (LPR) for detection of corrosion in post-tensioning (PT) components was investigated. The use of the electrical resistance (ER) technique, as well EIS and LPR, to detect air space corrosion at the grout voids was also explored. The results showed that high sensitivity noise measurements (in the μV range) are feasible for the strand-anchorage systems. The potential and galvanic current trends for the assemblies suggest the presence of activation-passivation cycles linked to each water ingress event. The EN method was adequate to identify only one modality of corrosion, and failed to detect other potentially important forms of corrosion despite the presence of significant macrocell current. In contrast, the EIS and LPR methods more reliably detected ongoing corrosion. The ER method could sensitively detect the deterioration of grouted and bare steel strands exposed to a high humidity environment as in the air space of a grout void. The air space corrosion experiments showed that an aggressive environment may evolve in the grout void, resulting in appreciable corrosion rates. Conceptual designs for field implementation of the above methodologies were formulated. A concept based on a robust, single element, single connection embedded steel probe, and another based on a two connection, single element embedded wire probe were considered to have the best combinations of features and ease of implementation. An alternative wire loop configuration is being tried in cooperative testing.

17. Key Words	18. Distribution Statement
Post-tensioning strand, grout, anchorage assemblies, recharge water, electrochemical noise, alternative corrosion detection methods	No Restriction. This report is available to the public through the NTIS, Springfield, VA 22161

19. Security Classif.(of this report)	20. Security Classif. (of this page)	21. No. of Pages	22. Price
Unclassified	Unclassified	71	

DISCLAIMER

The opinions, findings, and conclusions expressed in this publication are those of the authors and not necessarily those of the State of Florida Department of Transportation.

SI* (MODERN METRIC) CONVERSION FACTORS

APPROXIMATE CONVERSIONS TO SI UNITS

Symbol	When You Know	Multiply By	To Find	Symbol
		LENGTH		
in	inches	25.4	millimeters	mm
ft	feet	0.305	meters	m
yd	yards	0.914	meters	m
mi	miles	1.61	kilometers	km
		AREA		
in^2	square inches	645.2	square millimeters	mm^2
ft^2	square feet	0.093	square meters	m^2
yd^2	square yard	0.836	square meters	m^2
ac	acres	0.405	hectares	ha
mi^2	square miles	2.59	square kilometers	km^2
		VOLUME		
fl oz	fluid ounces	29.57	milliliters	mL
gal	gallons	3.785	liters	L
ft^3	cubic feet	0.028	cubic meters	m^3
yd^3	cubic yards	0.765	cubic meters	m^3
		NOTE: volumes greater than 1000 L shall be shown in m^3		
		MASS		
oz	ounces	28.35	grams	g
lb	pounds	0.454	kilograms	kg
T	short tons (2000 lb)	0.907	megagrams (or "metric ton")	Mg (or "t")
		TEMPERATURE (exact degrees)		
°F	Fahrenheit	5 (F-32)/9 or (F-32)/1.8	Celsius	°C
		ILLUMINATION		
fc	foot-candles	10.76	lux	lx
fl	foot-Lamberts	3.426	candela/m^2	cd/m^2
		FORCE and PRESSURE or STRESS		
lbf	poundforce	4.45	newtons	N
lbf/in^2	poundforce per square inch	6.89	kilopascals	kPa

APPROXIMATE CONVERSIONS FROM SI UNITS

Symbol	When You Know	Multiply By	To Find	Symbol
		LENGTH		
mm	millimeters	0.039	inches	in
m	meters	3.28	feet	ft
m	meters	1.09	yards	yd
km	kilometers	0.621	miles	mi
		AREA		
mm^2	square millimeters	0.0016	square inches	in^2
m^2	square meters	10.764	square feet	ft^2
m^2	square meters	1.195	square yards	yd^2
ha	hectares	2.47	acres	ac
km^2	square kilometers	0.386	square miles	mi^2
		VOLUME		
mL	milliliters	0.034	fluid ounces	fl oz
L	liters	0.264	gallons	gal
m^3	cubic meters	35.314	cubic feet	ft^3
m^3	cubic meters	1.307	cubic yards	yd^3
		MASS		
g	grams	0.035	ounces	oz
kg	kilograms	2.202	pounds	lb
Mg (or "t")	megagrams (or "metric ton")	1.103	short tons (2000 lb)	T
		TEMPERATURE (exact degrees)		
°C	Celsius	1.8C+32	Fahrenheit	°F
		ILLUMINATION		
lx	lux	0.0929	foot-candles	fc
cd/m^2	candela/m^2	0.2919	foot-Lamberts	fl
		FORCE and PRESSURE or STRESS		
N	newtons	0.225	poundforce	lbf
kPa	kilopascals	0.145	poundforce per square inch	lbf/in^2

*SI is the symbol for the International System of Units. Appropriate rounding should be made to comply with Section 4 of ASTM E380.

EXECUTIVE SUMMARY

Severe corrosion damage and even complete failure have been observed in external post-tensioned (PT) tendons of pillars or superstructure box segments of three Florida pre-cast segmental bridges over salt water. The failures occurred relatively early in their expected service life. Corrosion of strands is a particularly serious problem, as the integrity of the structure is dependent on the large tensile load concentrated by the tendon. Therefore, development of highly reliable and non-intrusive detection methods for PT anchorage corrosion is desirable to aid in revealing impending occurrences and implementing timely repair procedures. The methods should be suitable for practical implementation at multiple anchorage locations, eventual remote operation, and have the potential for being applied at moderate cost. The aim of the present work was therefore to determine the feasibility and sensitivity of the various electrochemical and related methods for corrosion detection in PT systems.

Specific tasks included (i) conceptual design and laboratory assessment for an Electrochemical Noise (EN) monitoring probe; (ii) evaluation of alternative conventional electrochemical techniques such as Linear Polarization Resistance (LPR) and Electrochemical Impedance Spectroscopy (EIS); (iii) assessment of the extent of corrosion that may exist in the air space of PT voids and formulation and assessment of conceptual designs to monitor that corrosion by means of available methods and (iv) formulate conceptual designs for practical field implementation of the methodologies found to be most successful in the previous tasks.

The feasibility of EN measurements in strand-anchor assemblies with simulated bleed water voids was demonstrated for both potential (ENP) and current (ENC) modalities. Simple embedded electrodes sufficed. High sensitivity (μV range) ENP measurements, necessary due to the large working electrode area, were achieved without need for highly sophisticated signal processing instruments.

Anchor assemblies were built with plain cement grout (P) and a proprietary low-bleed grout (S). The potential and galvanic current trends for both assemblies confirmed the presence of apparent activation-passivation cycles linked to water recharge events. In P assemblies water recharge events were concurrent with high amplitude EN signals, resembling those related to metastable pitting events. However, the water recharge events did not produce recognizable EN signatures for the S assemblies, despite the presence of a strong macrocell current. The lack of noise response in the S assemblies showed that EN technique may be limited to detecting adequately only some forms of corrosion in PT anchorages, leaving other potentially important corrosion modalities undetected.

Practical implementation of traditional EIS and LPR electrochemical corrosion measurements was demonstrated. In contrast to EN, the EIS and LPR methods reliably and sensitively detected ongoing corrosion and its detailed trends in all cases. The LPR method in particular showed good potential for practical implementation.

Simulated air-space corrosion experiments confirmed that an aggressive environment may evolve in the grout void even on strand wires covered with a residual hardened grout layer, resulting in corrosion rates that may have damaging effects in a relatively short service time. Electrical Resistance (ER) probes customized for PT anchor air space conditions were constructed, and their operability demonstrated. The functionality of Wire-Grout-Wire (WGW) probes for EIS and LPR measurements in PT anchor air space conditions was also demonstrated.

Nine conceptual designs for field implementation of the above methodologies were formulated. A concept based on a robust, single element, single connection embedded steel probe, and another based on a two connection, single element embedded wire probe were considered to have the best combinations of features and ease of implementation. Field trials for those concepts are proposed and cooperative activities are in progress.

TABLE OF CONTENTS

INTRODUCTION

Severe corrosion damage and even complete failure have been observed in external post-tensioned (PT) tendons of pillars or superstructure box segments of three Florida pre-cast segmental bridges over salt water [Sagüés, 2003; Wang, 2005a]. The failures occurred relatively early in their expected service life. The first incident was reported at the 18-year old Niles Channel Bridge (NCB) in Florida Keys [Powers, 1999; Sagüés, 2000] followed by the 7-year old Mid Bay Bridge (MBB) in the Western panhandle [Corven, 2001] and finally the 15-year old Sunshine Skyway Bridge (SSB) over Tampa Bay [FDOT, 2002]. The tendons in these structures consist of bundles with 19 or more seven-wire high strength (ultimate tensile strength 1.86 GPa (270 ksi)) steel strands encapsulated in a high-density polyethylene (HDPE) duct. The tendon is connected to an anchorage assembly, which includes wedges to hold the tendons that pass through an anchor head with tapered holes, transferring force to the concrete. Portions of the tendon pass through pipes in intermediate deviation blocks or U-bends to provide lateral force transfer where needed. After the strands have been tensioned, the space between the tendon and the anchorage (or ducts) is normally completely filled with cementitious grout to protect the steel against corrosion by providing a highly alkaline environment, which induces metal passivation. The grout also allows for some force transfer between strand and anchorage in case of strand breakage or loosening [Salas, 2004; Wang, 2005a].

Previous work [Powers, 2002; Wang, 2005a; Wang, 2005b] showed that bleed water formation when the mix water and the cement particles segregate (bleeding) during the grouting process [Ghorbanpoor, 1992] is a key factor in the development of corrosion. The bleed water tends to accumulate at the tendon high points where anchorages are commonly placed, forming voids there upon absorption of the water by the grout or evaporation through incomplete anchorage sealing. As indicated by some authors [Bricker, 2005], the bleed water itself can be very aggressive causing corrosion while the bleed water is still present. Corrosion can also occur at the region where the steel emerges from the grout into the void, either when the system is still wet from its original condition, or during later recharge events from external water intrusion into the voids at or near the anchorage [Wang, 2005b]. At the same time the high humidity environment inside the grout voids may induce atmospheric-like air space corrosion on the bare steel. Other detrimental factors such as decrease of grout pH in the voids due to concrete carbonation [Moreno, 1988], and galvanic coupling between strand steel and the ductile cast iron anchorage body [Powers, 2002] can considerably aggravate the corrosion. Additionally, because of evaporative chloride concentration the chloride content of pore water can increase to a level sufficient to cause the breakdown of passivity at the local pH and potential conditions [Li, 2001; Moreno, 1988].

In PT structures, the corrosion of steel tendons is a particularly serious problem, as the structural integrity of the bridges is dependent on the large tensile load concentrated by the tendon. Failure of a tendon, due to strand corrosion could have grave consequences. Therefore, development of highly reliable and non-intrusive

detection methods for PT anchorage corrosion is desirable to aid in revealing impending occurrences and implementing timely repair procedures. The methods should be suitable for practical implementation at multiple anchorage locations, eventual remote operation, and have the potential for being applied at moderate cost. The methods could supplement or even substitute other procedures presently used by FDOT (such as boroscope examinations and vibrational testing) that are either laborious, or have limited sensitivity, or can be applied only to external tendons.

In the above context, electrochemical techniques are appealing methods to detect the corrosion in PT anchorages since those techniques can be highly sensitive and can be applied to hidden components, as is the case of bonded tendons. Among these methods, electrochemical noise (EN) may be particularly desirable for early damage detection in PT tendons due to its high sensitivity to corrosion and instrumental simplicity if implemented as potential-EN, which is based on the measurement of open-circuit potential (OCP) fluctuations that develop in systems corroding actively. In such case, measurements can be conducted using a simple reference electrode even if it experiences long-term potential drift. EN may also identify the type of corrosion occurring in the system, particularly pitting corrosion [Cottis, 2001; Cottis, 2006], which is a common early deterioration mode of PT steels in anchorages or ducts. However, the small amplitude of the potential-EN signal due to the larger anchorage-strand area is a possible drawback for this technique. Therefore, other well established but more demanding electrochemical procedures such as electrochemical impedance spectroscopy (EIS) and linear polarization resistance (LPR) should be also considered. While EN, LPR and EIS are promising methods to detect corrosion at the grout-metal interface in the bulk of the grout or at the grout-air void boundary, those techniques may not be adequate to detect corrosion of strands fully in the air-space at the bleed void. That mode of damage may be important due to the high humidity potentially present in the void and chloride accumulation at the surface of the strands For that region, the use of the simpler electrical resistance (ER) method (based on the resistance increase resulting from the section thickness decrease of the corroded metal), as well as the use of conventional EIS and LPR with special test arrays, may hold promise and merit investigation.

The aim of the present work was therefore to determine the feasibility and sensitivity of the various electrochemical and related methods for corrosion detection in PT systems.

To address those objectives, activities were conducted in four areas:

1) Conceptual design for an EN monitoring probe, laboratory assessment of the EN modalities for steel corroding in anchorage assemblies, and evaluation of the reliability of EN for damage detection in PT tendons.

2) Evaluation of alternative conventional electrochemical techniques such as LPR and EIS to monitor the corrosion development in PT components.

3) Assessment of the extent of corrosion that may exist in the air space of PT voids and formulation and assessment of conceptual designs to monitor that corrosion by means of the ER, EIS, and LPR methods.

4) Formulate conceptual designs for practical field implementation of the methodologies found to be most successful in the previous tasks.

Activities keyed to those four areas are described in detail and keyed to each of the following sections.

Section 1: EVALUATION OF ELECTROCHEMICAL NOISE

In this portion of the investigation, the feasibility and sensitivity of the Electrochemical Noise method to detect corrosion in anchor-strand systems was evaluated.

Background

The traditional LPR methods measure the current transient when a small DC potential perturbation from the OCP (usually up to 10 mV) is applied to the system. This technique is easy to implement, but there are numerous complicating factors, such as, for example, electrolyte resistance (R_S) and interfacial capacitance (C_0), that can lead to miscalculation of the corrosion rates [Sagüés, 1995; Sagüés, 2006]. EIS is a powerful method for characterizing materials and their interface with electrolytes that can eliminate most of the artifacts affecting LPR. EIS consists basically of AC impedance measurement of the metal-electrolyte interface by applying a single frequency voltage (or current) with small amplitude to the interface and measuring the amplitude and phase shift of the resulting current (or potential) and repeating the process over a frequency range [Macdonald, 2005; Sagüés, 2006]. However, complexity in data interpretation remains an important drawback of this technique. Both EIS and LPR have an additional disadvantage, which is the requirement of having, at least, two embedded electrodes carefully positioned. Potential EN is arguably the simplest technique to implement because it is based on the measurement of the spontaneous short-term fluctuations in OCP and/or current which take place when a system is corroding [Cottis, 2001; Dawson, 1996]. Additionally, EN can be recorded with just one electrode, but in contrast to the conventional OCP measurement EN is nearly insensitive to aging drift of the electrode. All the electrochemical techniques described above have a major advantage over the weight loss method (WLM) or the electrical resistance method (ER, described in detail in Section 3) since the corrosion rates can be determined in minutes or hours while the WLM or ER need days or months [Dawson, 1996]. Despite the advantages of EN, the decrease of the noise magnitude with increasing specimen surface area [Arrieta, 2003] may restrict the usefulness of this procedure, especially for the strand-anchorage assemblies, which have a large surface area.

The most attractive characteristic of EN is its ability to detect pitting corrosion. EN signals corresponding to pitting corrosion are often characterized by individual transients with a rapid potential drop during the initiation and nucleation stages. In the simplest scenario this transient results from the accumulation of electrons at the metal surface due to the metal dissolution during a predominantly anodic initial stage, which terminates by pit repassivation or another anodic process [Arrieta, 2003]. After the repassivation, a predominantly cathodic stage takes place. This latter stage is characterized by slow exponential-like potential recovery and recharging of the double layer capacitance at the metal-electrolyte interface (Figure 1, p. 34). The pitting corrosion has a distinct time domain and spectral signature, which can be used in order to diagnose early corrosion activity. Mechanistic interpretations of the origin of EN vary,

but the phenomenology of EN provides often a distinct and useful indicator of corrosion activity.

The following details an investigation to determine the potential of EN for detecting corrosion in PT assemblies with bleed water voids. An implementation concept based on placing an activated titanium wire (as a short-term reference electrode) inside grouted anchorages is evaluated. The EN modalities for steel corroding in anchorage assemblies with two types of grout (representing materials used in earlier and present construction practice) were also determined.

Experimental Procedure

Two series of mock-up anchorage assemblies were constructed using actual ductile iron anchorage bodies and unstressed high strength eutectoid carbon steel strands (ASTM A416/A416M-98) as described in a previous report [Wang, 2005a]. Figures 2a and 2b (p.34) show configuration details. The series P assemblies (P1 to P3) used a plain cement grout with addition of a commercial aluminum based expansion agent. This type of grout was used in earlier construction practice, which did not effectively prevent the formation of bleed water voids. The series S assemblies (S1 to S4) used a new-generation commercial low-bleed grout representative of materials currently used.

The implementation concept involves a sensing probe consisting of mixed-metal oxide activated titanium wire (ATW) embedded in the grout inside the anchorage. In an actual application that arrangement could be achieved either by drilling into the grout in existing anchorages, or by casting in place for new construction. This approach has been successfully employed here to monitor EN of the system, as well as to measure LPR and EIS (described in Section 2). In this design, an ATW placed ~ 0.5 cm from the strand surface is used as reference electrode (RE) for EN potential measurements (ENP) and periodically calibrated against a saturated calomel electrode (SCE) with a Luggin-style sensing tip next to the embedded REs. ATWs were placed at various locations for future expanded testing, but this report concerns only results obtained with the ATW placed at location 8-1 in Figure 2. The strand bundle and anchorage were electrically connected through a closed external switch allowing macrocell current to flow. The anchor/strand galvanic current was periodically monitored by inserting a 0.1 Ω input resistance ammeter across the switch. A 10 Ω resistor was inserted between the strand bundle and anchor body to measure current EN (ENC), which are alternative measurements of electrochemical fluctuations, this time in the current flowing between two electrodes.

The spontaneous open circuit potential (OCP) as well as the galvanic current fluctuations of the interconnected strand-anchor systems were acquired by using a low noise voltage follower (VF) connected to a very low intrinsic noise 100X preamplifier circuit built at the University of South Florida and a Vernier^{TM} data acquisition interface with 12-bit resolution. A schematic of the EN acquisition system is shown in Figure 3

(p.35). The OCP was measured by connecting the strand-anchorage and the ATW to a voltage compensator (VC), which was used to remove the DC component by dialing the appropriate voltage. The DC compensated signal was fed into the VF and then into the 100X preamplifier circuit. The VF was used to effectively increase the input impedance of the system to > $1x10^{10}$ Ω. The output of the 100X preamplifier was connected to the Vernier instrumentation amplifier (IA). The selectable ranges of input voltage in the IA were usually set at ± 200 mV for ENP and at ± 20 mV for ENC. The VC was adjusted at the beginning of each 420 s EN recording interval to obtain a starting compensated potential close to the zero of the recording window. All the EN records were collected using battery operation to minimize aliasing effects [Cottis, 2006] observed in previous experiments (as illustrated in Figure 4, p. 35) due to electrical interference when the Vernier data acquisition interface was directly connected to the nearby data processing computer. The EN signals were collected in packets of 4200 data points at a rate of 10 Hz. After the experiment, the data stored in the Vernier interface were retrieved with the Logger Pro 2.2™ software to display the actual EN signals as a potential-time plot. The potential value indicated by the VC was manually recorded as the nominal OCP value for that EN record. When ENC was acquired, the potential value indicated by the VC corresponded to the galvanic current flowing in the interconnected anchorage-strand and the corresponding potential EN record was converted to a current EN record per Ohm's law.

In addition to battery operation of the acquisition unit, a careful shielding arrangement was designed and implemented to avoid spurious signals due to external noise. In this arrangement the anchor body was grounded by connecting to the negative terminal of the acquisition device and the reference electrode was connected to the live input (Figure 3). Polarity was inverted to report the results consistent with common use in the electrochemical literature.

Table 1 lists the Vernier data acquisition interface and system resolutions for the IA input voltage ranges used. The ultimate system resolution was 0.16 μV for the ± 20 mV input range, but in practice the system resolution for detection of electrochemical potential fluctuations was ~1 μV due to the intrinsic noise of the system, as shown in Figure 5 (p. 36). This system resolution meets the desired target resolution based on expected signal amplitudes, which are lowered because of the large metal area (~ 1,000 cm^2).

Periodically, 100 mL of fresh deionized water was added to the top of assemblies to simulate the effects of external moisture leaking into the anchorage as detailed by Wang [Wang, 2005a]. Moderate chloride contamination of the grout in the P group had taken place earlier [Wang, 2005a]. Galvanic current, potentials, and the corresponding EN signals were recorded before and after the water additions. All the experiments were performed at 23 ± 2 °C. All the potentials are reported in the SCE scale.

Results and Discussion

The open circuit potential (OCP) and the galvanic current trends of an interconnected strand-anchor system for the three P and the three S assemblies tested are shown in the Figures 6 (p. 37) and 7 (p. 38), respectively. In the P assemblies the fresh water addition caused a sharp potential drop of ~300 mV (occasionally preceded by a slight increase), to a minimum value of -0.38 V to -0.52 V after ~ 3 h. Afterwards the potential slowly recovered (over several weeks) toward its initial value. In the S assemblies a similar but slower drop was observed to a minimum of -0.52 V and -0.61 V after ~ 1 day. Recovery took place after several weeks.

Corresponding trends were observed for the galvanic currents (Figures 6b and 7b, positive values denote that the anchor body was the net anode). In all assemblies, macrocell currents were lower than 10 μA (anchor slightly anodic in the P assemblies, cathodic in the S assemblies) before the water recharge events. Upon water addition, the current increased considerably with the anchor as the anode, to maxima of 0.50 mA to 0.90 mA for the P series and 0.12 mA to 0.56 mA for the S series. In the P assemblies the anchor remained anodic, but the current dropped slowly reaching values < 10 μA after several weeks following a recharge event. In contrast, in all the S assemblies the macrocell current experienced a reversal to anodic strand behavior (usually 1 to 2 days after the initial maxima), reaching extremes of -0.20 mA to -0.28 mA after ~ 1 week and then recovering to pre-water addition values after several more weeks. As reported in previous work [Wang, 2005b], the potential and current trends indicate the presence of apparent activation-passivation cycles linked to each recharge event.

Figures 8 (p. 39-41) and 9 (p. 42-44) illustrate the effect of water recharge on ENP and ENC patterns of the P and S systems respectively. The EN time records are presented after removing the trend from the original voltage-compensated signal. This was done by fitting the experimental data to a quadratic trendline of the form, $y=at^2+bt+c$, where y is the fitted trendline, a, b, and c are constants and t is time in seconds. The fitted trendline was then subtracted from the measured signal. In all graphs, an arbitrary potential (current) zero was used for clarity; however the zero corresponds to the nominal values present just before the reported record, indicated in each graph. The EN pattern of the P assemblies changed drastically upon water addition (Figure 8). After water addition, noise events characterized by an abrupt decrease of potential (or increase of current) and a slow exponential-like recovery were clearly observed. The OCP events were ~ 0.3 to 1 s long with 10 to 100 μV amplitude. The duration of individual current noise events ranged from 0.1 to 1 s and the amplitudes, from 100 to 500 nA. The EN transients occurred randomly and were more frequent a short time after the water addition (~ 1 to 3 h). The rate of appearance and the magnitude of fluctuations decayed with time and after 2 days noise events were rarely observed. These noise fluctuations resemble those often related to metastable pitting corrosion events in carbon steel and aluminum alloys [Cottis, 2001; Cottis, 2005]. EN signals corresponding to metastable pitting show usually individual transients with a

sharp drop of potential during the nucleation stage, which can be interpreted as being caused by an initial predominantly anodic phase where the metal dissolution produces an accumulation of electrons at the metal surface. In this interpretation, the anodic stage terminates suddenly due to pit repassivation and is followed by a cathodic stage, with a slower exponential recovery of potential caused by recharging of the double layer capacitance [Arrieta, 2004; Sasaki, 2002]. The decrease with time of the event rate is commonly observed, for example by Uruchurtu et al. [Uruchurtu, 1987] for pure aluminum constantly submerged in 3.5 wt% NaCl solution. In the present case the decay may be simply associated with lesser availability of electrolyte as the recharge water dissipates, but it may also reflect exhaustion of pitting sites [Uruchurtu, 1987].

In contrast with the P assemblies, the EN patterns for S assemblies did not change significantly upon water addition as exemplified in Figure 9. Noise events like those of the P systems were rarely observed in the S series, even when they were experiencing an appreciable level of galvanic current.

The amount of metal dissolved and the nominal size of the pit ascribed to a typical noise event can be estimated, under certain assumptions, from the height of the potential step experienced in such event and the interfacial capacitance of the metal-electrolyte interface [Arrieta, 2003]. It is assumed that the event consisted of an abrupt anodic initial fall in potential followed by a slower cathodic increase. It is also assumed that each event corresponds to an individual pit. In this case, the pit size can be calculated by the following equations:

$$q = C_a \, \Delta V \qquad [1]$$

$$m = \frac{\frac{q}{q_e z}\overline{M}}{N_{Av}} \qquad [2]$$

$$r_p = \left(\frac{3m}{2\pi\rho} \right)^{1/3} \qquad [3]$$

where q is the charge released in an individual event, C_a is the interfacial capacitance for the anodic stage, ΔV is the size of the potential step in a single event, m is the mass of metal loss in a single event, r_p is the radius of the pit (assuming an hemispherical shape) associated to the single noise event, ρ is the density of the corroding metal (7.87 g/cm^3), q_e is the elementary charge (1.6 $\times$ 10^{-19} C), z is the number of electrons transferred per ion, N_{Av} is the Avogadro constant (6.02 $\times$ 10^{23}) and $\overline{M}$ is the atomic weight of the corroding material (56 g/mol). For the current noise, the pit size can be determined simply calculating the charge in an individual event, $I\Delta t$, and applying equations [2] and [3]. The effective system area may be approximated as being 1,000 cm^2 (in the order of the area of anchorage metal in contact with grout, plus the area of the envelope of the strand bundle in the upper region of the assembly), and the effective

interfacial capacitance as being 100 $\mu F/cm^2$, in the order of values often reported for steel in concrete. With those assumed parameter values, the amount of charge estimated for the largest events in Figure 8 corresponded to a pit size in the order of 6 μm for the ENP and 2 μm for the ENC, a plausible value for these systems.

Analysis of EN in the frequency domain by computing the Power Spectrum Density (PSD) has been commonly used to monitor corrosion [Arrieta, 2003; Uruchurtu, 1987]. EN time records are converted into their corresponding frequency spectra by using the Discrete Fourier Transform (DFT), normally in the form of Fast Fourier Transform (FFT) algorithms. The PSD is then calculated from the DFT results, as the squared amplitudes of the sine waves, divided by the frequency separation and has units of V^2/Hz or A^2/Hz [Arrieta, 2003; Cottis, 2001].

Typical potential and current PSD plots for P and S systems are shown in Figures 10 (p. 45) and 11 (p. 46), respectively, before and after water addition. The resulting roll-off slopes (S_r) are shown in Table 2 and 3 for P and S assemblies. It is noted that the time constant of the high frequency cut-off circuit in Figure 3 was only 0.01 s, so it does not play a significant role in the frequency response determinations considered here, which are for $f < 5$ Hz. S_r values were estimated by a trendline of the form $k_s f^{\alpha}$, corresponding to PSD in f range of 0.05 to 1 Hz. The S_r in db/decade is then obtained from the exponent (α) as follows [Arrieta, 2003]:

$$S_r = 10\,\alpha \qquad [4]$$

The experimental potential S_r were found to be between ~ -16 and -22 db/decade for P assemblies (Table 2) and between ~ -21 and -25 db/decade for S assemblies (Table 3). The current S_r ranged from ~ -13 to -17 db/decade for P assemblies (Table 2) and from ~ -14 and -18 db/decade for S assemblies (Table 3). The water addition did not affect significantly the S_r in both P and S systems. However, the potential and current PSD for P assemblies increased by a factor of ~ 100 and ~5, respectively, upon water addition, tending to recover the original value after ~ 2 to 3 days. The pre-water recharge potential and current PSD for S assemblies were ~ 10 times and ~ 2 times, respectively, lower than the PSD for P assemblies and did not change upon water recharge. These results are in good agreement, as expected, with the trends observed in the EN time records. The S_r of potential and/or current has been proposed as an indicator of the corrosion type. However, there is large variability in the literature for the values of S_r assigned to the different corrosion modes, and S_r in the same order as those calculated for the P and S assemblies have been variously associated with uniform and pitting corrosion [Arrieta, 2003; Cottis, 2001]. Therefore, corrosion modes cannot be distinguished reliably only on the basis of S_r.

From an instrumentation standpoint, the results showed that high sensitivity (e.g. 1 μV range) ENP measurements could be effectively conducted in full size anchorages when EN developed (P assemblies). Sensitivity to small signals is required because the large strand-anchorage surface area lowers the amplitude of ENP [Arrieta, 2003; Arrieta, 2004]. In the case of the P assemblies the typical ENP event amplitude was

only in the order of 10-100 μV and the background signal between events was in the order of only 10 μV, but practical observations were conducted routinely. The S assemblies had no EN activity detectable with the available sensitivity, suggesting that equipment not normally available for practical applications would be required in such case. The equipment demands for detecting ENC are less stringent because ENC is expected to increase with system area. In the present case sensitivity in the order of 20 nA was enough to characterize the behavior of the P assemblies.

The cause for the virtual lack of observable noise in the S assemblies has not yet been identified. It could be thought that the higher baseline resistivity of the grout used in the S series (~ 10 times greater than those of P series after completely cured) [Sagüés, 2003] may have reduced corrosion severity and consequently EN levels, but the S assemblies had actually higher macrocell currents than in the P systems. Moreover, after the successive events simulating water leakage the strand to anchor grout resistance for both P and S assemblies were found to be comparable. The results suggest that the corrosion in the P assemblies was more localized, pitting-like, than in the S assemblies. In that context it is worth noting that the moderate, 500 ppm native chloride content of the S grout [Sagüés, 2003] may not have been enough to promote strong corrosion localization, compared to the case of the P assemblies to which salt water had been added in earlier experiments [Wang, 2005b]. That chloride may have further concentrated at the anchor body-grout interface and/or at the grout-void interface of the strand bundles in the P assemblies with greater EN manifestations.

Regardless of the cause, the lack of appreciable noise response in one class of assemblies despite strong corrosion macrocell activity indicates an important drawback in the use of EN as a sole method for early corrosion detection method in these systems. Consequently, other electrochemical procedures less corrosion-mode specific such as electrochemical impedance spectroscopy (EIS) and linear polarization resistance (LPR) have been also explored for this purpose, as shown in the following section.

SECTION 2: EVALUATION OF ALTERNATIVE CONVENTIONAL ELECTROCHEMICAL TECHNIQUES - EIS AND LPR

This section examines the suitability of Electrochemical Impedance Spectroscopy (EIS) and the simpler Linear Polarization Resistance (LPR) technique to detect corrosion of metal in contact with bulk grout post-tensioned anchorages that have bleed-water voids and are subject to periodic water intrusion.

Experimental Procedure

To conduct the EIS and LPR tests, the same test assemblies as for the EN measurements were used with the same plain grout and a proprietary grout conditions. A classical three electrode configuration was employed with the anchor-strand system as the working electrode (WE), the embedded ATW as the reference electrode (RE), and a mixed-metal oxide activated titanium rod, which was placed parallel to the strand bundle, as the counter-electrode (CE). The EIS and LPR experiments were performed before and after the water recharge events using a Gamry PCI-4 Potentiostat from Gamry Instruments, Warminster, U.S.A. The EIS tests were conducted at OCP with signal amplitude of 10 mV RMS in the frequency range from <1 mHz to 100 kHz. The numerical fitting programs Gamry Echem Analyst™ (Gamry Instruments, Warminster, U.S.A.) or Zview2™ (Scribner Associates, Inc., Southern Pines, U.S.A.) were used to estimate the electrochemical parameters. The LPR measurements started from the OCP toward an overpotential of –10 mV (cathodic direction). A scan rate of 0.1 mV/s was used.

Results and Discussion

The experimental results showed that both LPR and EIS methods are promising approaches to detect corrosion, even if it does not have a noise signature, in the anchor-strand systems. Figures 12 (p. 47) and 13 (p. 47) show the EIS behavior of a P grouted assembly before and after a water recharge event. Comparable results were obtained in the replicate P and in the other S assemblies for this and the other observations described below.

To determine the electrochemical parameters, the system was idealized as a constant phase element (CPE), where Y_{0ID} and n_{ID} are the CPE parameters, in parallel with an idealized polarization resistance (R_{PID}). The solution resistance (R_S), which corresponds to the grout resistance, is in series with the parallel combination. The value of R_S was obtained by fitting the impedance predicted by such analog circuit to the actual impedance results, considering all data in the 1 mHz to 100 Hz frequency interval. The fitting algorithm under those conditions is biased to the preponderance of data relevant to R_S at the highest frequencies and yields a well defined estimate of the grout resistance. The overall impedance behavior usually deviated somewhat at the highest frequencies from the idealized system assumed. That situation, combined with

the data weighing procedures used in the fitting algorithm tended sometimes to result in misleading results in the value of R_P yielded by the fit procedure, as much of the spectral information for that parameter is contained at the lower frequencies and in a relatively small data population. Consequently, a compromise procedure was developed that consisted in first obtaining provisional estimate values R'_P and R'_S by performing the fit only for the 10 lowest frequency data (using frequencies <1mHz when available) in the impedance spectrum obtained. Thus, the calculated low-frequency real axis intercept, not affected by high frequency spectral features was $R'_P + R'_S$. Subtracting from that sum the previously (and reliable) value of R_S yielded an improved estimate of the polarization resistance $R_P = R'_P + R'_S - R_S$. That R_P value is the one reported below and used in subsequent calculations. The values of Y_0 and n obtained with the 10-point low frequency data fit are also those reported subsequently. Figure 13 exemplifies the results (solid line) of the provisional fit and estimate of R'_P (as well as Y_0 and n) for a P1 assembly after water recharge. The figure also illustrates how the high-frequency real intercept of the provisional estimate is slightly higher than the value for the smallest absolute phase angle (which corresponds to a frequency ~ 100 Hz), hence the independent determination of R_S to refine the overall estimate of R_P.

In the periods before the first water recharge, or after the effects of water recharge had dissipated, the low frequency impedance data for either grout type in most cases (with exceptions noted later) did not converge toward a recognizable finite value of R_P, as exemplified in Figure 12. The correspondingly large value of R_P returned by the curve-fitting procedure was consequently subject to great relative uncertainty. Thus, calculated values of R'_P >~ 10^4 Ω were treated as being infinity, as illustrated in Figure 12.

The results of the model fitting are shown in the Figures 14-17 (pp. 48-51) for all assemblies. For clarity an arbitrary time is indicated in the diagrams, in which the first recharge water event would correspond to the starting point. The corrosion currents I_{corr} estimated by the Stern-Geary relationship [Mansfeld, 1976a] below, with an assumed Stearn-Geary constant value of 26 mV (treating the reactions in the system as if they were under simple activation polarization) are shown in the same Figures. The 1 μA lower limit in the graph is a placeholder for negligible I_{corr} values (infinity R_P as indicated above).

$$I_{corr} = \frac{0.026V}{R_P} \qquad [5]$$

A nominal corrosion rate can be calculated (assuming a nominal area of 1000 cm^2, which is in the order of the total amount of metal surface in contact with grout for the dimensions of the strand-anchor assembly) according to the following equation:

$$Corrosion\ rate\,(\mu m/y) = \frac{I_{corr}\, m_{eq}\, 3.15\times 10^{11}}{A\,\rho\, 96500} \qquad [6]$$

In equations [5] and [6] the corrosion current in A, the assembly ferrous components are treated as pure Fe, m_{eq} is the equivalent weight of Fe (27.92 g/equivalent), A is the nominal area in cm^2 and ρ is the density of Fe (7.87 g/cm^3).

As shown in Figures 14-17 a dramatic decrease in R_P (and a proportional increase in I_{corr}) by a factor in the order of ~10^2 to >10^3 for both assemblies was observed upon water recharge events. Reflecting the wetting, the grout solution resistance R_S decreased somewhat for the P systems and markedly (~4 to 10 times) for the S systems. Upon water addition the Y_0 parameter increased abruptly too (~10 times) in all S assemblies suggesting the development of a larger area of effective contact between the metal surface and the electrolyte. This behavior however was seldom observed in the P assemblies. Those results suggest that, in the absence of excess water, electrolytic contact between the grout and the metallic surfaces in the S assemblies was poorer than in the P assemblies. Wang [Wang 2005a] noted in previous tests that in some of the test assemblies thin gaps had developed between the grout and the anchor body, so the observed effects may reflect the recharge water temporarily filling some of the gaps. For either grout type there was no clear correlation between the water recharge events and the n parameter, except for the suggestion of a slight increase of the latter upon recharge.

As shown by comparing Figures 14 and 16, the S assemblies had upon water recharge higher I_{corr} values (typically ~2 mA, maximum ~7 mA) than the P assemblies (~0.5 mA, maximum ~2 mA). For the assumed nominal total corroding area of 1,000 cm^2 those values correspond to nominal corrosion rates in the order of ~25 μm/y (maximum of ~80 μm/y) for the S assemblies and ~6 μm/y (maximum of ~25 μm/y) for the P assemblies. Moreover, for the S assemblies I_{corr} remained appreciable for longer times; 30 weeks after the recharge event I_{corr} values of ~20 μA (corresponding to a nominal 0.2 μm/y) were still observed. In contrast, the I_{corr} values for the P systems were again undetectable 5 to 15 weeks following the recharge event. The generally higher corrosion rates found in the S group are not apparently associated with the relative R_S values, since the S assemblies had larger pre-wetting R_S values than those of P assemblies (in the order of ~ 10 Ω and ~ 3 Ω respectively). Upon water recharge the R_S values for both P and S systems became comparable, but I_{corr} was larger in the S systems as noted above.

The I_{corr} trends were consistent with the relative galvanic current and potential trends noted earlier, both on the overall values and in the way in which the recharge event effects persisted with time. In Figure 18 (p. 52) the I_{corr} value estimated by EIS each time a test was performed, and the simultaneous measured value of the macrocell current ($I_{macrocell}$, reported in Figures 6 and 7) are compared for both assemblies. The diagonal line corresponds to a hypothetical 1:1 agreement between both values. A clear correlation of increasing $I_{macrocell}$ with increasing estimated I_{corr} was observed over about 2 orders of magnitude for both types of assemblies and with comparable values within replicate specimens. The trends were distinctly below the 1:1 lines so that in general, I_{corr} was ~2 to 4 times and ~4 to 10 times greater than $I_{macrocell}$ for P and S assemblies, respectively. The overall pattern and value of the ratios are reasonable as the $I_{macrocell}$

can never be greater than the total local cell action current, since the former results only from imbalance of the latter. The value of the ratios is in keeping with common observations of corrosion of steel in concrete and modeling predictions [Kranc 1994]. It is noted however that while $I_{macrocell}$ was evaluated by direct measurement, the value of I_{corr} stems from modeling assumptions of the impedance response and assumptions on the value of kinetic parameters. Thus, the value of the ratio between those magnitudes is subject to modeling/assumption uncertainty and interpretation of that value is limited to the above observation that on average it is in a plausible range.

LPR measurements were conducted over the same general time frame as the EIS tests, and the I_{corr} values estimated by LPR (LPR-I_{corr}) and by EIS (EIS-I_{corr}) are compared in Figure 19 (p. 53) for both types of assemblies. As in Figure 18, the diagonal line corresponds to a hypothetical 1:1 agreement between both values. To determine the LPR-I_{corr} values a refined R_P (LPR-R_P) was used. The LPR-R_P values were compensated for R_S and for the presence of interfacial CPE behavior using the corresponding parameters obtained from the EIS measurements. The compensation was made by first subtracting an amount equal to $I \bullet R_s$ from the potential V at each point of the measured current (I) - V curve obtained in the LPR test, thus obtaining an ohmic resistance-compensated curve I-V_{comp}. The correction for the current demanded by the CPE was done by the following relationship [Sagüés, 1995; Sagüés, 2006]:

$$R_P = \left[\frac{1}{R_a} + \frac{Y_0 \, S^n V_{max}^{\ -n}}{\Gamma(1-n)} \right]^{-1} \qquad [7]$$

where V_{max} is the maximum compensated potential applied, S is the scan rate (0.1 mV/s), Γ is the Euler´s Gamma function, and R_a is the apparent R_P determined by the slope at $V=V_{max}$ of the I-V_{comp} curve, and Y_0 and n are the CPE parameters obtained from the impedance experiment performed usually 6 to 10 h before. It is noted that the correction represents only a first approximation as it does not take into consideration the convolution resulting from the simultaneous presence of the R_S and the CPE [Sagüés, 1995].

Figure 19 shows general agreement between the EIS-I_{corr} and LPR-I_{corr} trends when EIS-I_{corr} was higher than 10 μA. The ratios between LPR-I_{corr} and EIS-I_{corr} in those cases were ~ 1 to 2 and ~ 1 to 1.5 for P and S assemblies, respectively. When EIS-I_{corr} decreased several weeks after the recharge event, the ratios became larger (ratios > 30 occurred for both assemblies if EIS-I_{corr} was small enough), likely reflecting uncertainty as noted earlier in determining R_P (and consequently I_{corr}) when it is very large. Nevertheless, the results show that the simpler LPR technique can detect ongoing corrosion in these assemblies, and reveal the sudden increase of the corrosion rates upon water intrusion.

Both polarization techniques as well as the macrocell current measurements usually indicated higher corrosion rates in the S group, even though salt water was never added there. Those results support the concern that the native chemical

composition of this proprietary low-bleed grout may create a more corrosive environment upon external leakage than otherwise. Such concerns have been noted by Bricker [Bricker, 2005] and Wang [Wang 2005a], the latter in connection with the presence of relatively high, but still meeting specifications, native chloride content of the grout. This issue should be examined in detail in future work.

It is recognized that application of the conventional techniques examined here involves numerous assumptions and simplifications, so accurate determination of corrosion rates is not obtained. However, the techniques provide clear indication of the onset of active corrosion and approximate numerical indicators of its severity suitable for an early warning system. Regardless of the factors responsible for the observed corrosion, the above results demonstrated the ability of both LPR and EIS methods to detect corrosion in post-tensioning tendons, in one case when EN had been unable to do so. From the point of view of practical deployment the LPR technique would be preferable since this method is simpler to implement than EIS because of less demanding data acquisition and processing needs. The approach illustrated here to process the LPR data assumed that some EIS testing had already taken place, since R_S, n and Y_0 values were used in the calculations. The need for such prior determination can be obviated with a compromise approach. Such approach would involve, in the case of R_S, conducting a simple single-frequency test (for example at ~100 Hz, with instrumentation similar to a Nilsson™ soil resistivity meter) and building such test into the instrumentation and testing protocols, thus keeping instrumental complexity to a minimum. The correction for Y_0 and n may be conducted, as an approximation, using generic values of those parameters obtained separately from similar systems such as those used in the present investigation.

SECTION 3: DETECTION OF AIR SPACE CORROSION AT GROUT VOIDS

This section addresses the feasibility of detecting air space corrosion in tendon anchorages by the EIS, LPR, and ER methods. The ER is a corrosion monitoring method based on the principle of an increase in electrical resistance produced by a decrease in the section thickness of the metal when it corrodes [Moran, 2006; Oung, 1997]. Weight loss measurements were also conducted for comparison.

Experimental Procedure

Atmospheric corrosion test chambers (Figure 20, p.54)) were designed and constructed. Relative humidity (RH) was controlled by introducing in the cell 1 L of saturated- or 89 g/L- sodium chloride solution for 75% RH or 95% RH respectively [Mansfeld, 1976b, Young, 1967]. EIS, LPR and ER experiments were performed with duplicate specimens at 23 $\pm$ 2 °C. The gravimetric tests had greater multiplicity. The 75% RH humidity chamber was only used for weight loss experiments and preliminary ER tests.

For the EIS and LPR measurements two 5 mm diameter steel wires (10.5 cm long) extracted from an actual high strength strand were used to build wire-grout-wire (WGW) probes (Figure 21, p.54)). After removing the mill scale, both wires were attached parallel to each other with a 0.6 mm or 1 mm gap between them. Plastic spacers at the end of the probes kept the two wires electronically isolated from each other. Thin stainless steel wire contacts were spot welded at the end of each wire for external connection. The probes were immersed in a fluid 0.42 water/cement ratio grout (type 1 Portland cement) and then lifted forming upon curing a thin grout layer on the surface and across the gap. The grout layer in the 1 mm gap probes was thicker than in the 0.6 mm gap probes, which were made in a different batch. The grouted probes were cured in a 100% RH chamber for a day and then placed in the 95% RH chamber. EIS measurements of the WGW probes were carried out at OCP with 10 mV RMS amplitude in the frequency range from 100 kHz to 10 mHz to determine polarization resistance and corrosion currents of the probes. The LPR experiments were conducted at 0.1 mV/s, starting from the OCP to an overpotential of 10 mV in the cathodic direction. Both experiments were performed using Parstat™ 2263 from Princeton Applied Research, Oak Ridge, U.S.A. and Gamry™ PCI-4 from Gamry Instruments, Warminster, U.S.A potentiostats. The reference and counter-electrode were connected to one wire of the probe and the working electrode to the other one, so the impedance measured corresponded to the wire-grout-wire series combination. The electrochemical parameters were estimated by using the programs Gamry Echem Analyst™ from Gamry Instruments, Warminster, U.S.A or Zview2™ from Scribner Associates, Inc., Southern Pines, U.S.A.

The ER probes were designed as a Wheatstone bridge with one branch isolated from the corrosive environment. The ER probes consisted of two identical, 120 cm long plain low carbon steel rebar tie wires, 1.60 mm diameter, in the “as-received” condition

(dark mill scale on the metal surface). One of the wires, the working element, was exposed to the atmosphere inside the chamber. The other wire, the reference element, was protected by sealing it inside the probe body (PVC pipe) from the external medium (Figure 22, p. 55). The covered wire provides a reference for evaluating changes in the uncovered wire and also serves to compensate for the effects of temperature changes on resistance. In the final design, both internal and external wires were double-coiled to minimize inductance effects. External wires of some ER probes were also covered by a grout film to simulate the conditions at the tendon anchorage. The grout was the same type as that used for the WGW probes.

The corrosion rate of the exposed wire was calculated by using the ratio of the exposed wire resistance to that one of the covered wire over time and accounting for the wire initial dimensions. A 60 Hz AC, 80 mA excitation current was created with a 21 V output transformer in series with a 260 Ω resistor and the probe. The resistance of each wire was ~0.8 Ω, resulting on only ~10mW total probe power dissipation, a negligible amount of heat production rate considering the dimensions of the probe.

The probes were made part of a Wheatstone bridge as shown in Figure 23 (p.56), where R1 and R2 are arms of an external potentiometer adjusted initially to match the resistance ratio of the probe wires. A ~0.03 μF capacitor (value selected by trial and error) was placed across R2 until there was nearly zero phase shift across the V_{out} terminals. Without that capacitor a small phase shift, due to the mutual inductance of the internal and external coiled wires, was present which prevented obtaining a sharp null during initial adjustment. The initial resistance ratio, R_{out} / R_{in} (see Figure 23), of the probe was nearly 1. From that initial condition, when the wire corrodes the resistance increases by a factor of (1+P). P is a function of the input voltage (V_{in}) and V_{out}, according to the relationship below [Dally, 1993].

$$P = \frac{4V_{out}}{V_{in} - 2V_{out}} \qquad [8]$$

The corroding wire radius (r_{corr}) can, thus, be calculated by the following equation:

$$r_{corr} = r_o \cdot \sqrt{1/(1+P)} \qquad [9]$$

where r_0 is the radius of the wire estimated at the beginning of the measurement.

The system imbalance sensitivity was improved to 0.005 mV, corresponding to a detectable change of corroding wire radius in the order of 1/4000 (0.2 μm).

A LabView™ program (Figure 24, p.57) was developed to determine P by measuring V_{out} and V_{in} of the bridge. The program measures simultaneously the supply AC voltage and the voltage across the bridge from which the resistance of outer branch can be calculated. The program consists of three parts. The first part configures the

data acquisition board and converts binary counts to engineering units. The second part performs voltage measurements and the third part analyzes the data and calculates P, displayed in the front panel of the program display (Figure 24a). The data acquisition board used for this task was an USB-1608FS from Measurement Computing, with a 16-bit precision (0.03 mV resolution error). The sampling rate was set to 24000 samples/s and the number of samples to 6000.

The weight loss experiments were conducted with bare and grouted wires (20 helically shaped outer wires extracted from actual 7-wire steel strands from the same stock used for P and S the assemblies, and 8 steel low carbon steel tie wires as used for the ER probes). The helically shaped wires were 0.508 cm in diameter and 35 cm long; the steel tie wires were 0.16 cm in diameter and 46 cm long. Before and after the test, the specimens were cleaned per ASTM G1 and then weighted on 10^{-3} and 10^{-4} grams precision balances, respectively. Some of the specimens were grouted by dipping as for the other tests, and cured for 2 days inside a 100% RH chamber before introducing in the 95% RH chamber.

Results and Discussion

The WGW electrochemical probe system can be approximated as behaving as the equivalent circuit in Figure 25a (p. 58), where C_i are CPEs representing the interfacial capacitance of the metal-grout interface of each wire, R_P is the polarization resistance of that interface, and C_s and R_s represent, respectively, the dielectric capacitance and ohmic resistance of the grout bridge, the former of which was found to be not negligible for the system and frequency range examined. For simplicity the two metal-grout interfaces were assumed to behave similarly. Thus, the measured impedance could be represented by a single C_m – R_m parallel combination as shown in Figure 25b, where $R_m=2R_P$ and C_m is a CPE with parameters $Y_{0m}=Y_0/2$ and n.

The EIS behavior of WGW probes exposed to the 95% RH environment had general features similar to those of the mock-up assemblies, but with a better defined additional high frequency semicircle in the impedance diagram as illustrated in Figure 26 (p. 59). As discussed above, the first semicircle corresponds to R_S and C_S, while the second is related to R_m and C_m. Because the grout resistance-capacitance component has a very short time constant, the analysis to determine the circuit parameters relevant to the polarization of the corrosion reactions was limited to the frequency interval 10 mHz to 1 Hz, where the effect of C_s is small[1]. Thus, the equivalent circuit used for the actual EIS data analysis had R_S, R_m and C_m as the only fit parameters and the results in the following are discussed in terms of the parameter values for one of the interfaces.

The R_S and the R_P trends for the 1 mm gap electrochemical probes exposed to 95% RH environment are shown in the Figure 27a (p. 60). Upon initial exposure to 95%

[1] A few of the tests revealed a more complex spectrum, with two time constants in the low frequency regime. In those cases, only a restricted range of frequencies at the low end of the spectrum (from ~100 mHz to 10 mHz) was used for analysis. The cases involved were for days 39,42,64,94 and 208 in WGW0 and for days 229-264 in WGW4.

RH the R_S and the R_P values were small, but then increased drastically tending to stabilize after ~50 days. The increase in R_s likely reflects the establishment of a less interconnected pore network in the grout as curing matures. Figure 27b shows that the values for R_P in the 0.6 mm probes were in the same order as those for the 1mm probes, but not as stable. The values of R_s were about one order of magnitude greater than those for the 1 mm gap probes and less stable as well.

A typical LPR potential-current curve of a 1 mm gap WGW probe is shown in Figure 28 (p. 61). As pointed out in Section 2, an apparent polarization resistance can be obtained from the terminal slope at the maximum potential and a refined estimation was obtained using equation [7] following the same procedure described earlier. Figure 29 (p. 62) shows comparable relative trends for the R_P values estimated by LPR and EIS methods for both the 1 mm and 0.6 mm gap probes, but the R_P obtained from LPR tended to be lower than those ones from EIS by about a factor of 2. It is noted that comparable ratios between EIS-R_P and LPR-R_P were observed for the P and S assemblies (Fig. 19; note that there the comparison is made in term of I_{corr}, which is inversely proportional to R_P).

Corrosion current I_{corr} values were calculated by the Stearn-Geary relationship (equation [5]) as detailed in Section 2, but assuming that both wires were corroding equally and the individual polarization resistances were in series) and reporting the result as the I_{corr} for one of the two wire-grout interfaces in the probe after making the appropriate correction. The corresponding nominal corrosion rates were estimated per equation [6] assuming an area of 8 cm^2 for the metal in effective contact with grout on each of the probe wires. That area value was estimated by making the rough assumption that all the excitation current flows through the one-half of the wire perimeter facing the other wire. The time evolution of I_{corr} for both types of WGW probes is shown in Figure 30 (p. 63). The I_{corr} values were, in general, larger in the first days of exposure but after several days decreased to ~ 0.3 μA and ~ 0.1 μA for 1 mm and 0.6 mm gap probes, respectively. The I_{corr} for 0.6 mm gap probes were less stable than those of the 1 mm gap probes, reflecting the instability of the estimated R_P values noted before. While there is considerable uncertainty in the effective area of these specimens and from the other simplifying assumptions used, the results suggest that corrosion rates estimated by this method were in the order of ~ 0.3 μm/y.

The cumulative (i.e. averaged from the beginning of exposure until an exposure time t) corrosion rate of ER probes in μm/year was determined by:

$$CR = \Delta r \cdot 365/t \qquad [10]$$

where Δr is the radius change of the corroding wire in μm ($r_{initial}$ - r_{corr}) and t is the exposure time in days.

An instantaneous (actually short interval) corrosion rate can be calculated by evaluating equations [9] and [10] using the short interval Δt between two measurements, and using the first measurement as the initial condition.

The instantaneous and cumulative corrosion rate trends for grouted and bare ER probes exposed to the 95% RH environment are shown in the Figures 31 and 32 (p.64). Higher corrosion rates were observed in the first days of exposure especially for the bare steel probes but after 50 days the rates for both conditions reached a plateau of ~5 μm/y. The fluctuations of the instantaneous corrosion rate may be attributed to the resolution of the individual measurements and/or minor temperature and RH fluctuations. The cumulative corrosion rates for ER probes had comparable decreasing trends. After 98 days the cumulative corrosion rates were 12 μm/y and 24 μm/y for grouted and bare ER probes respectively, reaching, after 196 days, 8 μm/y and 15 μm/y.

The weight loss measurements yielded results comparable to those of the ER probes as illustrated in Figure 33 (p. 65). After 98 days of exposure the average corrosion rate for grouted and bare helically shaped wires were 11 μm/y and 12 μm/y respectively, and 10 μm/y and 11 μm/y after 196 days. The average corrosion rate for bare steel tie wires was ~ 13 μm/y after 98 and 196 days of exposure.

In the 75% RH chamber none of the specimens examined experienced measurable corrosion rates, so that condition served as a baseline control. The result is consistent with the expectation that exposure at 75% RH does not meet the conditions necessary to trigger atmospheric corrosion. For bare metals that condition is typically encountered above 85% RH [Griffin, 2006], consistent with the present results.

The ER probes and weight loss measurements showed evidence that at 95% RH the corrosion rates were considerably higher than those of anchor-strand systems before water addition but usually smaller than the values obtained right after simulated recharge events. That ranking is to be expected from the relatively thin effective electrolyte layer present on the metal surface in the air space case. The grout film was not particularly protective, as shown by similar corrosion rates in the bare steel and grouted specimens. Tests after long exposure with pH paper and sprayed phenolphthalein on the grout film on probes in the 95% RH chamber indicated a near neutral pH, meaning that the thin layer of hardened grout had eventually carbonated in the chamber environment. Thus, the grout no longer had passivating properties to the steel and it is not surprising that measurable corrosion was taking place. This was further confirmed by direct observation of rusting on ER, weight loss and even some of the WGW probe wires.

The observation of rust on some WGW probe wires clearly indicated that significant corrosion was taking place. However, even though still greater than those in the mock-up anchorages before water recharge, the WGW apparent corrosion rates were one order of magnitude lower than those obtained by ER or weight loss. This discrepancy may be attributed in part to uncertainty in estimating the effective probe area in contact with grout. That area may be much less than the nominal assumed value because of cracks in the grout or disbondment at the grout-metal interface, thus greatly underestimating the actual rates over the remaining area of contact. Another

likely cause of insensitivity would be that the assumption of equal electrochemical behavior at the two metal-grout interfaces in a probe is wrong. If corrosion were to start at only one of the interfaces with the other largely in the passive condition, then the total series impedance would still be very large and the corresponding apparent current density would stay low until both wires are simultaneously in the active condition.

The worst-case surface-averaged corrosion rate values observed in the high humidity chamber (about 10 μm/y), if sustained over 10 years would correspond to an average loss of diameter of 100 μm, or about 8% reduction in cross-sectional area in a 5 mm diameter wire. Such a loss may already be considered of concern even if it were uniform, considering that one decade is a relatively short time compared to typical design life goals. As corrosion is likely to show some degree of localization, critical loss of strength could occur even earlier. Thus, these findings highlight air space corrosion as a potential cause of strand failure.

The same caveats noted in the previous section as to accuracy of the methods investigated apply here as well. The tests nevertheless showed that ER probes can detect instantaneous and cumulative corrosion loss with good sensitivity for both grouted and bare steel strands exposed to the simulated air void environment, if high relative humidity conditions exist. The interpretation of the WGW probe results needs to be refined to better assess their usefulness. The probes ER have promisingly good functionality but are of relatively large size, which poses an implementation constraint. A less sophisticate alternative would be the use of a thick wire loop or loops that could serve as a reference and counter electrodes for LPR measurements and also provide a simple pass-fail indicator of ongoing corrosion by regular simple continuity tests. Those and other possible variants are discussed in the next Section.

SECTION 4: CONCEPTUAL DESIGNS FOR IMPLEMENTATION

General requirements

The findings from the previous sections permit discerning advantages and disadvantages of various possible alternatives for implementation of early warning corrosion detection systems for PT anchorages. In the following, it will be assumed that the anchorage is for a tendon containing multiple (e.g. 17, 27, etc) 7-wire strands of sizes in the order of 0.5 in or 0.6 in, with a metallic wedge plate eventually covered by a concrete pourback, and with a metallic body. It will be assumed that a connection to the metallic body of the anchor can be readily made, and that the anchor is electrically grounded.

A key condition for any detection system is that it is robust enough to withstand normal construction handling during assembly, driving of the strands, and force jacking, and also any stresses generated by the fluid grout flow while pumping it in place. The probes must also be small enough to fit in the anchorage space without interfering with strand positioning and to prevent direct electric contact with the strands. In addition, the probes must necessitate only a minimum of electric contacts and be simple enough for economic construction and reliable operation when placed in large numbers.

The following design concepts address only the dimensional and materials issues, and not electronic instrumentation, since the latter can be adapted from existing technology as demonstrated in the previous sections.

One of the most challenging issues in implementing electrical or electrochemical probes in an anchorage concerns the number of needed insulated electric connections, as those are made most practically through the crowded wedge plate. Thus the systems will be classified by the number of independent contacts needed. In most cases at least one of the connections can be made through the anchorage ground and that feature is used to advantage.

It will be assumed that connections are implemented through one or more unused wedge sockets in the wedge plate, to permit use of available hardware without costly modifications or potential loss of strength. In such case, an unused socket plug is replaced by a plastic conical fitting with one or more separate wires running through it. Other openings such as unused vent holes can also be used to advantage. Custom insulated feedthroughs are possible through alterations of the wedge plate design, but at greater cost and design constraints.

All probes are assumed to be installed so the probe element is placed in the upper part of the anchorage where a bleed water void is more likely.

The following concept listing is not exhaustive but addresses the main capabilities of interest.

Single - Connection Concepts

S1 - Single element EN probe.

Design: Probe consists of a 1/8 in diameter activated Ti rod of the type used as temporary reference electrode in concrete [Castro, 1996]. The rod is integral with the external contact and feeds through into the anchor for as long as practical (e.g. 4 to 12 in) without creating a short circuit to the strands or anchor body.

Functionality: The probe serves as an EN reference electrode to detect corrosion, and also as a rod-to-ground two-point *ac* resistance probe to reveal presence of voids by showing greater resistance than that of peer assemblies. Probe may also detect corrosion by revealing potential drop of steel, compared with peer assemblies.

Advantages: Simple, economical, robust, only one connection needed.

Disadvantages: As shown in Section 1, EN may not always detect ongoing corrosion. If probe is fully in void EN measurement with probe is not possible. Long term stability of electrode potential may give misleading indication of corrosion condition.

S2 - Single element EIS-LPR steel probe.

Design: Probe consists of 1/8 in diameter steel rod, integral with the external contact and feeds through into the anchor for as long as practical (e.g. 4 to 12 in) without creating a short circuit to the strands or anchor body.

Functionality: The corrosion of the probe itself is detected; probe serves as surrogate for the strand-anchor system to detect corrosive conditions. Corrosion is measured by performing 2-point EIS or LPR measurements with probe as working electrode (WE) and strand-anchor as a counter electrode (CE) - reference electrode (RE) combination. That arrangement is workable because the combined surface area of the strand-anchor is much larger than that of the probe, so the impedance of the probe dominates.

As in Concept S1 the steel rod can serve also as a rod-to-ground two-point *ac* resistance probe to reveal presence of voids by showing greater resistance than that of peer assemblies. Also as in Concept S1 the probe may also detect corrosion if an unusually high potential difference develops between probe and ground, indicating that either one is corroding if the other is not.

Possible EN functionality.

Advantages: Simple, economical, robust, only one connection needed.

Disadvantages: If probe is fully in void polarization measurement of probe is not possible. If both probe and strand-anchor are corroding no telltale difference in potential may appear.

S3 - Single insulated contact wire loop.

Design: Probe consists of 1/16 in diameter steel wire (as in rebar tie wire), integral with the external contact and feeds through into the anchor continuing for a practical length (e.g. 4 to 12 in) bent as needed so as not to create a short circuit to the strands or anchor body in its free length, terminating spot-welded to the inside of wedge plate.

Functionality: The corrosion of the probe itself is detected; probe serves as surrogate for the strand-anchor system to detect corrosive conditions. Corrosion is detected only by break in wire due to full corrosion penetration and loss of electric continuity.

Advantages: Simple, economical, robust, only one connection needed. Very high reliability, very simple to monitor. Can detect air space corrosion.

Disadvantages: Lower sensitivity than other methods. No EN or potential measurement capabilities.

Dual - Connection Concepts

D1 - CE-RE EIS-LPR probe

Design: Probe consists of two 1/8 in diameter activated Ti rods, one short (e.g. 2-in) to serve as a RE and another long (e.g 12 inch) to serve as a counter electrode. Both electrodes are fed through one insulating wedge plug, or separately through two plugs if there is not enough room in one.

Functionality: Corrosion is measured by performing 3-point EIS or LPR measurements with strand-anchor as the WE. Either rod can serve also as a rod-to-ground two-point *ac* resistance probe to reveal presence of voids by showing greater resistance than that of peer assemblies. Either rod may also detect corrosion by revealing potential drop of steel, compared with peer assemblies. Possible EN functionality.

Advantages: Simple, economical, reasonably robust.

Disadvantages: If RE or WE fully in void, measurement not possible. Long term stability of electrode potential may give misleading indication of corrosion condition.

D2 - WE-RE EIS-LPR probe

Design: Same as D1, but long electrode is a steel rod.

Functionality: The corrosion of the steel wire itself is detected; wire serves as surrogate for the strand-anchor system to detect corrosive conditions. Corrosion is measured by performing 3-point EIS or LPR measurements with strand-anchor as the CE, short activated titanium rod as RE, steel rod as WE. Either rod can serve also as a rod-to-ground two-point *ac* resistance probe to reveal presence of voids by showing greater resistance than that of peer assemblies. Either rod may also detect corrosion by revealing potential drop of steel, compared with peer assemblies. Possible EN functionality. Possible macrocell current functionality by monitoring current between rod and rest of assembly if it is chosen to connect probe to assembly through a low resistance ammeter.

Advantages: Simple, economical, reasonably robust, somewhat more reliable R_P measurement than with system S2.

Disadvantages: If RE or WE fully in void, measurement not possible. Long term stability of electrode potential may give misleading indication of corrosion condition. Little gain over Concept S2 at cost of requiring one additional connection.

D3 - WGW probe

Design: Similar to that described in Section 3. Dual-wire probe may need shortening to avoid contact with anchor body or strands; thin wire connections may be needed to feed through to outside of anchor; probe cannot be inserted from outside.

Functionality: The corrosion of the dual steel wire assembly itself is detected; probe serves as surrogate for the strand-anchor system to detect corrosive conditions. Corrosion is measured by performing 2-point EIS or LPR measurements between wires, but can be adapted to perform 3-point tests using one of the wires as a RE, the other as CE and the strand-anchor assembly as WE. Either rod can serve also as a rod-to-ground two-point *ac* resistance probe to reveal presence of voids by showing greater resistance than that of peer assemblies. Either rod may also detect corrosion by revealing potential drop of steel, compared with peer assemblies. The dual wire assembly would still work as air space probe if it would end up entirely in void area. Possible EN functionality. Possible macrocell current functionality.

Advantages: Economical, able to monitor air space corrosion.

Disadvantages: Most important, as pointed in Section 2, if one of the wires corrodes and the other remains passive, an erroneously low corrosion rate would be estimated. Complicated and with critical dimensions; cannot be inserted from outside, potentially fragile.

D4 - Dual insulated contact wire loop.

Design: As in S3 but both wire ends free by means of dual feedthrough.

Functionality: The corrosion of the probe itself is detected; probe serves as surrogate for the strand-anchor system to detect corrosive conditions. Corrosion is detected by break in wire due to full corrosion penetration and loss of electric continuity. Alternatively, corrosion can be measured too by performing 2-point EIS or LPR measurements with probe as WE and strand-anchor as a CE-RE combination. Possible EN functionality. Possible macrocell current functionality.

Advantages: Simple, economical, moderately robust. Dual function, combining high sensitivity of EIS-LPR with very high reliability and ease of use of wire break method. Can detect air space corrosion.

Disadvantages: Similar to those noted for S2 and S3 for each respective mode of operation.

D5 - ER Probe

Design: Similar to that described in Section 3, but customized to fit space by using smaller diameter wire and coil forms, and with one wire termination spot-welded to wedge plate so it can operate with only two connections. Probe cannot be inserted from outside with that configuration. Possible adaptations of Corrosometer™ tubular ER probes may be feasible for compact design and external insertion, but losing sensitivity to pitting corrosion.

Functionality: As described in Section 3. May also serve as wire break probe.

Advantages: Can detect air space corrosion and measure it with high sensitivity. Dual functionality for wire break method and associated advantages.

Disadvantages: Complicated construction, cannot insert from outside, potentially fragile. No EN or potential measurement capabilities.

Triple - Connection Concepts

T1 - ER Probe

Design: Similar to D5, but with all three connections free by use of triple external feedthrough.

Functionality: As for D5, but able to perform polarization and EN measurements as well as 2-point resistance to ground and potential measurements. Possible macrocell current functionality.

Advantages: Multiple functionality as described for Concept D4.

Disadvantages: Complicated construction, cannot insert from outside, potentially fragile, three external connections needed.

Trial Implementation - Cooperative Activity

In a cooperative activity with the California D.O.T. (Caltrans), it single-contact wire loops per concepts developed under this project were installed in four anchorage heads at cantilevers under construction at the San Francisco-Oakland Bay Bridge (SFOBB), Westbound Skyway Structure. That structure is part of the SFOBB East Span Seismic Safety Replacement Project. A single wire loop was installed at each of Cantilever/Tendon locations E7W/C06N, E7W/C06S, E5W/B10S and E5W/B6S. Those wires will be monitored periodically to monitor corrosion conditions in those anchorages.

Summary

Selection of the best methodology for deployment will depend on specific project needs including number of units to be monitored, expectations of environmental aggressiveness, resources available, and sophistication of data acquisition and processing equipment available. Methods with the lowest number of required connections and easiest probe insertion are most appealing, in the absence of extensive prior experience. At present, methods S2 and D4 appear to be among the most promising considering the combination of simplicity of implementation and chances of success in early detection of ongoing corrosion. Deployment of those two methods on a limited trial basis is recommended for a suitable upcoming FDOT construction project. Additional cooperative activities with other transportation agencies, as illustrated above, should be pursued as well.

OVERALL PROJECT CONCLUSIONS

1) The feasibility of electrochemical noise (EN) measurements in strand-anchor assemblies with simulated bleed water voids was demonstrated for both potential (ENP) and current (ENC) modalities. Simple embedded electrodes sufficed. High sensitivity (μV range) ENP measurements, necessary due to the large working electrode area, could be achieved without need for highly sophisticated signal processing instruments.

2) Anchor assemblies were built with plain cement grout (P) and a proprietary grout (S).The potential and galvanic current trends for both assemblies confirmed the presence of apparent activation-passivation cycles linked to water recharge events. Sizable (e.g. 100 μA range) corrosion macrocell currents developed upon those events between the strand and the anchor components.

3) In P assemblies water recharge events were concurrent with high amplitude EN signals, resembling those related to metastable pitting events. However, the water recharge events did not produce recognizable EN signatures for the S assemblies, despite the presence of a strong macrocell current.

4) The lack of noise response in the S assemblies showed that EN technique may be limited to detecting adequately only some forms of corrosion in PT anchorages (e.g those were pitting is predominant), leaving other potentially important corrosion modalities undetected.

5) The feasibility of practical implementation of traditional electrochemical corrosion measurements such as Electrochemical Impedance Spectroscopy (EIS) and Linear Polarization Resistance (LPR) in strand-anchor assemblies was demonstrated. In contrast to EN, the EIS and LPR methods reliably and sensitively detected ongoing corrosion in the circumstances examined.

6) The EIS and LPR measurements successfully documented the onset of corrosion, the strength of the corrosion reactions, and the time evolution of corrosion before and after simulated recharge events. The results also were consistent with the expected relative magnitude of macrocell and total corrosion currents in the system.

7) There was good correlation between EIS and LPR measurements showing that the latter, simpler method has good potential for practical implementation.

8) Simulated air-space corrosion experiments showed that an aggressive environment may evolve in the grout void even on strand wires covered with a residual hardened grout layer, resulting in corrosion rates that may have damaging effects in a relatively short service time.

9) Electrical Resistance (ER) probes customized for PT anchor air space conditions were constructed and their operation with readily available electronic instrumentation was demonstrated. The probes showed adequate sensitivity to detect the corrosion rates of interest, and the results were validated against direct gravimetric measurements.

10) Wire-Grout-Wire (WGW) probes for EIS and LPR measurements in PT anchor air space conditions were constructed and their operation with readily available electronic instrumentation was demonstrated. However, sensitivity may be low and the interpretation of the WGW probe results needs to be refined to better assess their usefulness.

11) Nine conceptual designs for field implementation of the above methodologies were formulated. The listing is non-exhaustive as variations incorporating features of one or more concepts are possible. The implementation features deemed most important were the number of required external connections and mechanical simplicity.

12) A concept based on a robust, single element, single connection embedded steel probe, and another based on a two connection, single element embedded wire probe were considered to have the best combinations of features and ease of implementation. Field trials for those concepts are proposed and cooperative activities are in progress.

REFERENCES

Arrieta, I., “The Effect of Surface Area on Electrochemical Noise of Aluminum Alloys 1100, 2024 and 5052 in Chloride Media,” Thesis for M.Sc. in Chemical Engineering, University of South Florida, 2003.

Arrieta, I., Sagüés, A. A., and Joseph, B., paper No. 04456, Corrosion/2004, NACE International, Houston, TX, 2004.

Bricker, M. D., Schokker, A. J., “Corrosion from Bleed Water in Grouted Post-Tensioned Tendons”, R&D Serial No. 2547, Portland Cement Association, Skokie, Illinois, USA, 2005.

Castro, P., Sagüés, A. A., Moreno, E. I., Maldonado, L., and Genesca, J., "Characterization of Activated Titanium Solid Reference Electrodes for Corrosion Testing of Steel in Concrete", Corrosion 52, p. 609, 1996.

Corven, J., “Mid Bay Bridge Post-Tensioning Evaluation,” Final Report, Florida Department of Transportation, Florida, October, 2001.

Cottis, R. A., “Interpretation of Electrochemical Noise Data”, Corrosion 57, p. 265 (2001).

Cottis, R. A., paper No. 06432, Corrosion/2006, NACE International, Houston, TX, 2006.

Dally, J. W., Riley, W. F., McConnell, K. G., “Instrumentation for Engineering Measurements”, 2nd Ed., John Wiley & Sons, Inc., Hoboken, NJ, 1993

Dawson, J. L., “Electrochemical Noise Measurement: The Definitive In-Situ Technique for Corrosion Applications?”, Electrochemical Noise Measurement for Corrosion Applications, ASTM STP 1277, Kearns, J.R., Scully, J.R., Roberge, P.R., Reichert, D.L. & Dawson, J.L., Eds., American Society for Testing and Materials, p. 3, 1996.

FDOT (Florida Department of Transportation), “Sunshine Skyway Bridge Post-Tensioned Tendons Investigation,” February, 2002.

Ghorbanpoor, A., Madathanapalli, S. C., “Performance of Grouts for Post-Tensioned Bridge Structures,” Report FHWA-RD-92-095, Federal Highway Administration, Washington, DC, 1992.

Griffin, R. B., “Corrosion in Marine Atmospheres,” in Corrosion: Environments and Industries, ASM Handbook Vol. 13c, pp. 42-60, ASM International, Materials Park, OH, 2006.

Kranc, S. C. and Sagüés, A. A. "Computation of Reinforcing Steel Corrosion Distribution in Concrete Marine Bridge Substructures", Corrosion 50, p. 50, 1994.

Li, L., Sagüés, A. A., Corrosion 57, p. 19 (2001).

Macdonald, J. R., “Impedance Spectroscopy – Theory, Experiment, and Applications”, 2nd ed., John Wiley & Sons, Inc., New Jersey, 2005.

Mansfeld, F., “The Polarization Resistance Technique” in Advances in Corrosion Science and Technology, Vol. 6, M. G. Fontana and R. W. Staehle, Eds., Plenum Press (1976a).

Mansfeld, F., Kenkel, J. V. “Electrochemical monitoring of atmospheric corrosion phenomena,” Corros. Sci. 16, p. 111 (1976b).

Moran, G. C., Labine, P., “Corrosion Monitoring in Industrial Plants Using Nondestructive Testing and electrochemical Methods,” Ann Arbor, MI 2006.

Moreno, E. I., Sagüés, A. A., “Carbonation-Induced Corrosion of Blended-Cement Concrete Mix Designs for Highway Structures,” paper no. 636, CORROSION/98, NACE International, Houston, 1998.

Oung, J. C., Shih, H. C., Corrosion Prevention and Control 44, p. 173 (1997).

Powers, R. G., “Corrosion Evaluation of Post-Tensioned Tendons on the Niles Channel Bridge,” Florida Department of Transportation, Florida, June 29, 1999.

Powers, R. G., Sagüés, A. A., Virmani, Y. P., “Corrosion of Strand-Anchorage System in Post-Tensioned Grouted Assemblies,” in Proc. 17th U.S.-Japan Bridge Engineering Workshop, held Nov. 12-14, 2001, p. 579, Japan: Public Works Research Institute, 2002.

Sagüés, A. A., Kranc, S. C., Moreno, E., Corrosion Science 37, p. 1097 (1995).

Sagüés, A. A., Kranc, S. C., Hoehne, R. H., “Initial Development of Methods for Assessing Condition of Post-Tensioned Tendons of Segmental Bridges,” May, 2000.

Sagüés, A. A., “Lectures Notes on Electrochemical Impedance Spectroscopy for Corrosion Testing”, University of South Florida, 2006.

Sagüés, A. A., Powers, R. G., and Wang, H., Paper No. 03312, Corrosion/2003, NACE International, Houston, 2003.

Salas, R. M., Schokker, A. J., West, J. S., Breen, J. E., and Kreger, M. E., “Conclusions, Recommendations and Design Guidelines for Corrosion Protection of Post-Tensioned Bridges,” Report FHWA/TX-04/0-1405-9, Texas Department of Transportation, Texas, February, 2004.

Sasaki, K., Levy, P. W., and Isaacs, H. S., Electrochem. Solid-State Lett. 5, p. B25 (2002).

Uruchurtu, J. C., and Dawson, J. L., Corrosion 43, p. 19 (1987).

Wang, H., Sagüés, A. A., “Corrosion of Post-Tensioning Strands,” Final Report BC353-33, Florida Department of Transportation, Florida, November 1, 2005a.

Wang, H., Sagüés, A. A., and Powers, R. G., “Corrosion of the Strand-Anchorage System in Post-Tensioned Grouted Assemblies”, Paper No. 05266, Corrosion/2005, NACE International, Houston, 2005b.

Young J. F., “Humidity control in the laboratory using salt solutions - A Review,” J. Appl. Chem. 17, 241 (1967).

TABLES

Table 1. Vernier data acquisition interface system resolution for the IA input voltage ranges.

Range (mV)	Actual Vernier interface Resolution[1] (μV)	Ultimate System Resolution[2] (μV)	Nominal System Resolution[3] (μV)
± 20	16.1	0.16	0.097
± 200	143	1.43	0.97

[1] The actual Vernier interface resolution corresponds to the minimum potential step directly discernable in an actual potential record.

[2] The ultimate system resolution corresponds to the resolution of the Vernier interface connected to the 100X preamplifier circuit, i.e. the actual Vernier resolution divided by 100. As noted in the text, intrinsic system noise is several times greater than this minimum discernable step.

[3] The nominal system resolution is the nominal Vernier interface resolution, which is the range (40 mV for the ± 20 mV setting, for example) divided by 4096 (a 12-bit device can distinguish one in 4096 parts of its range), when connected to the 100X preamplifier. In this case, the nominal Vernier resolution should be divided by 100. However, the interface software utilizes only about 2/3 of the total range, with the result shown.

Table 2. S_r and k_s estimated for P1 assembly.

	Potential PSD		**Current PSD**	
time	**k_s**	**S_r**	**k_s**	**S_r**
before water addition	2.10^{-13}	-18.6	8.10^{-17}	-16.0
5 h to 12 h after	2.10^{-11}	-18.5	4.10^{-16}	-16.1
2 to 4 days after	6.10^{-13}	-21.1	6.10^{-17}	-15.5
2 weeks after	4.10^{-13}	-20.5	5.10^{-17}	-14.5

Table 3. S_r and k_s estimated for S4 assembly.

	Potential PSD		**Current PSD**	
time	**k_s**	**S_r**	**k_s**	**S_r**
before water addition	2.10^{-14}	-23.1	3.10^{-17}	-17.2
1 day after	6.10^{-14}	-22.6	3.10^{-17}	-16.8
5 day after	4.10^{-14}	-23.0	3.10^{-17}	-14.0

FIGURES

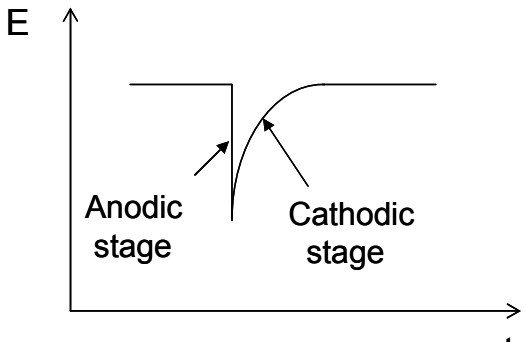

Figure 1. Noise transient showing the anodic and cathodic process [Arrieta, 2003].

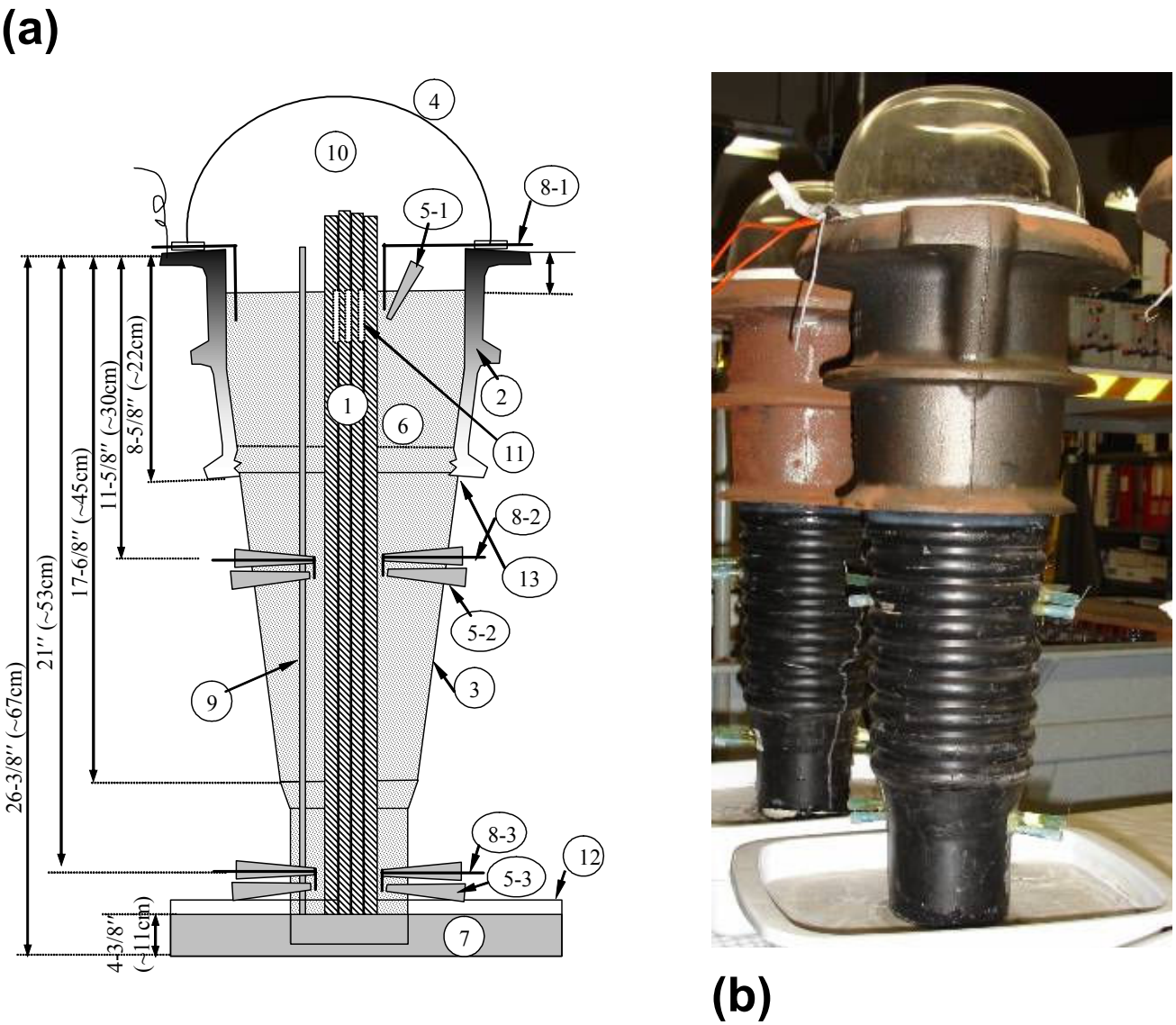

Figure 2. Schematic (a) and picture (b) of anchor test assembly [Wang, 2005a]
1. 7 PT strands bundle 2. Cast-iron anchor 3. HDPE trumpet 4. Glass vessel 5-1,2,3. Potential ports at top, middle, and bottom, respectively 6. Grout 7. Base built using cement Paste 8-1,2,3. Ti wire reference electrodes at top, middle, and bottom, respectively 9. Ti Counter electrode 10. Void
11. Interstrands void if present 12. Plastic pan 13. Joint of plastic trumpet and anchor

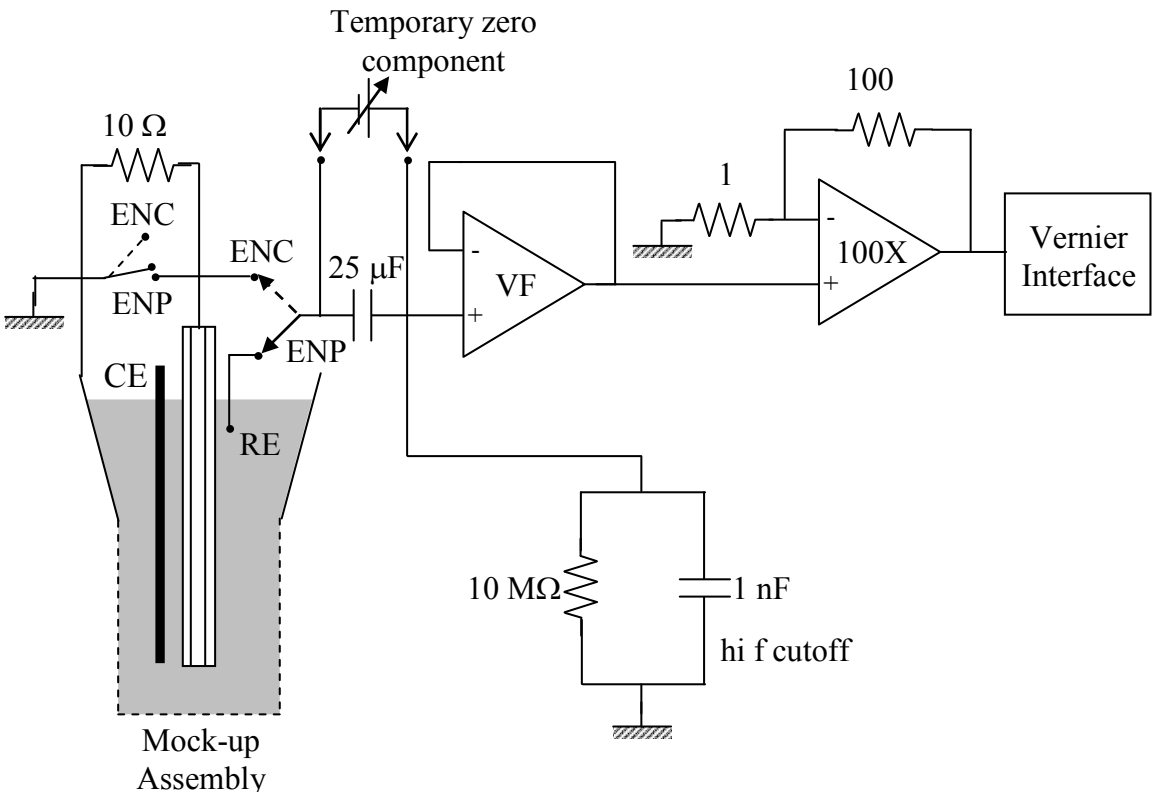

Figure 3. Schematic of experimental setup.

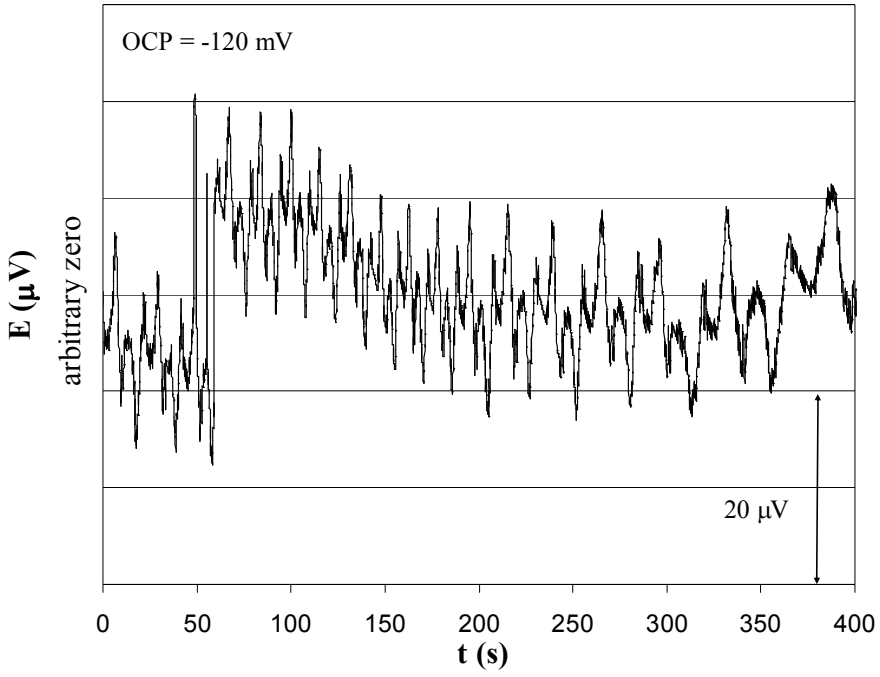

Figure 4. OCP signal of the anchor-strand system for P3 assembly showing aliasing effect due to electrical interference. Subsequent experiments were conducted using battery operation to avoid this problem.

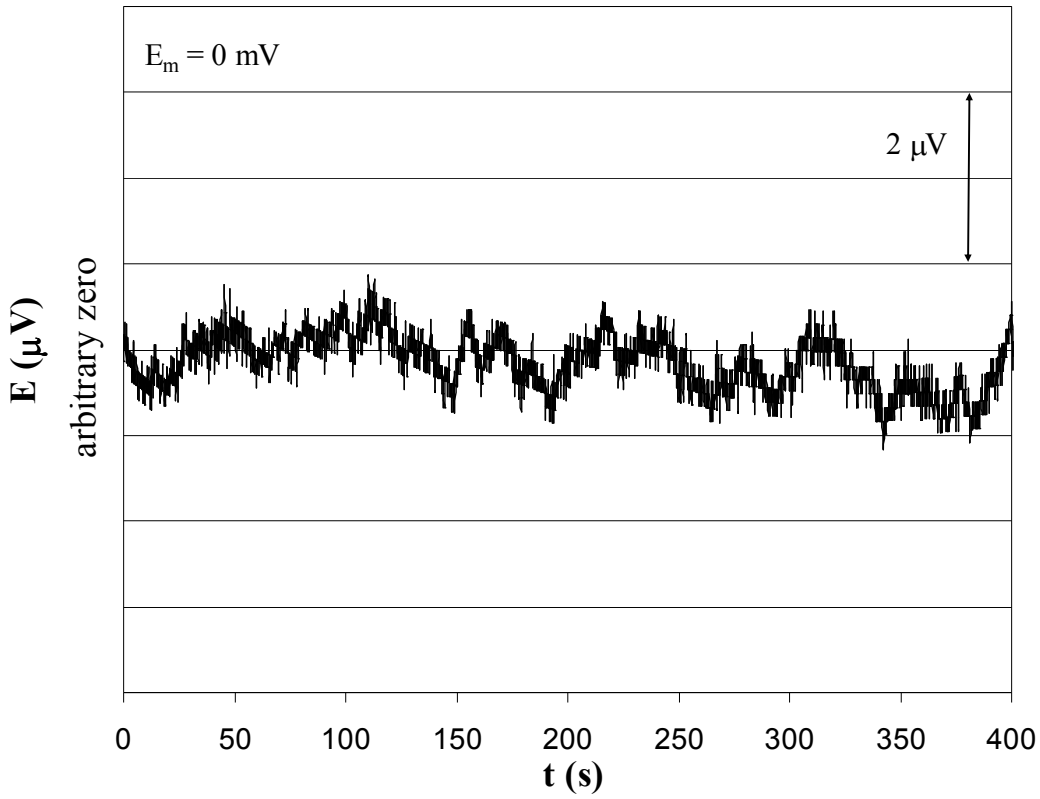

Figure 5. Intrinsic noise of the measuring system. The EN record was acquired by short-circuiting the acquisition device. The potential range of the Vernier acquisition system was ± 20 mV. The effective overall potential scale is indicated in the graph.

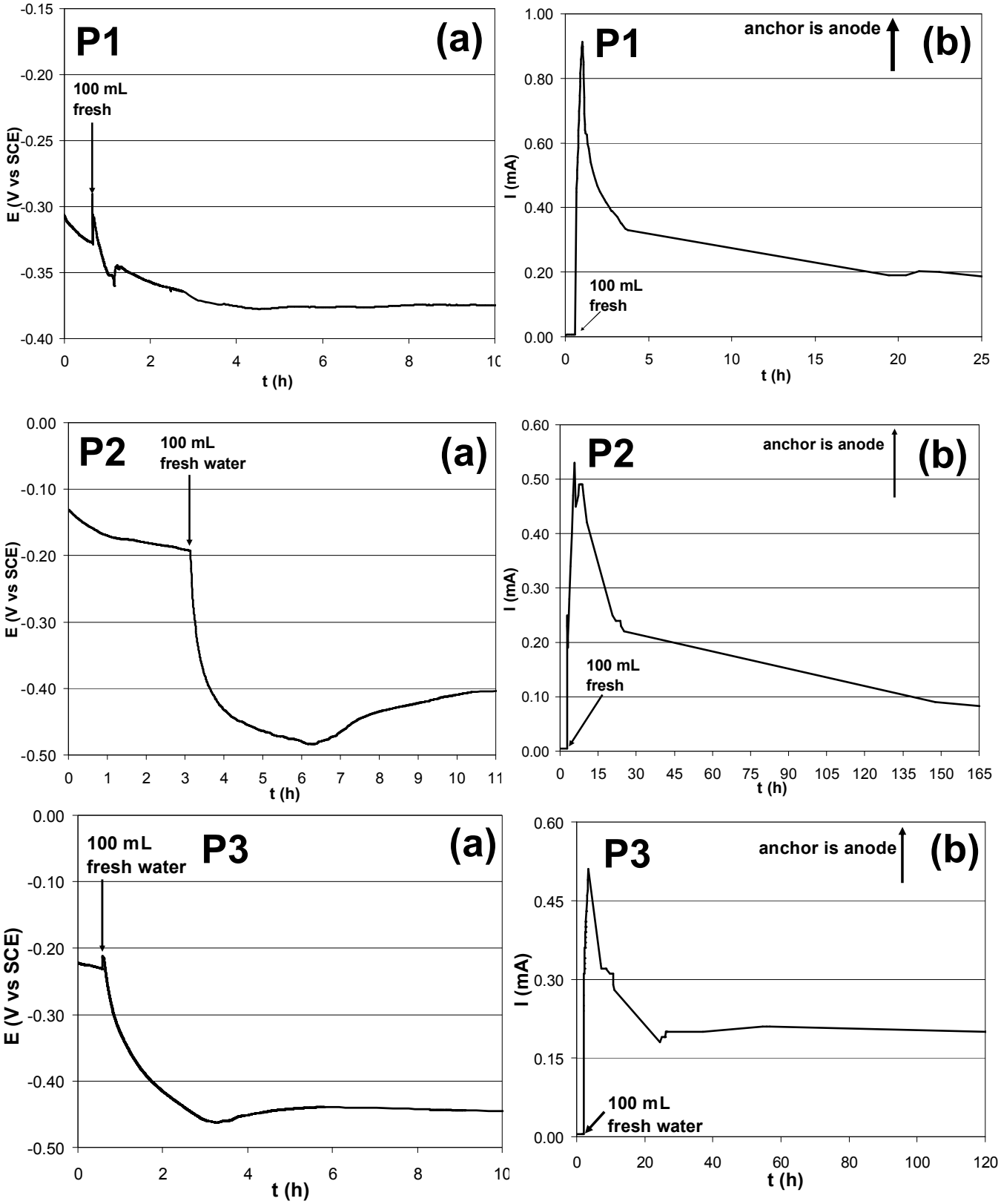

Figure 6. Potential (a) and current (b) trends of anchor-strand system for P assemblies (the arrow indicates the water addition).

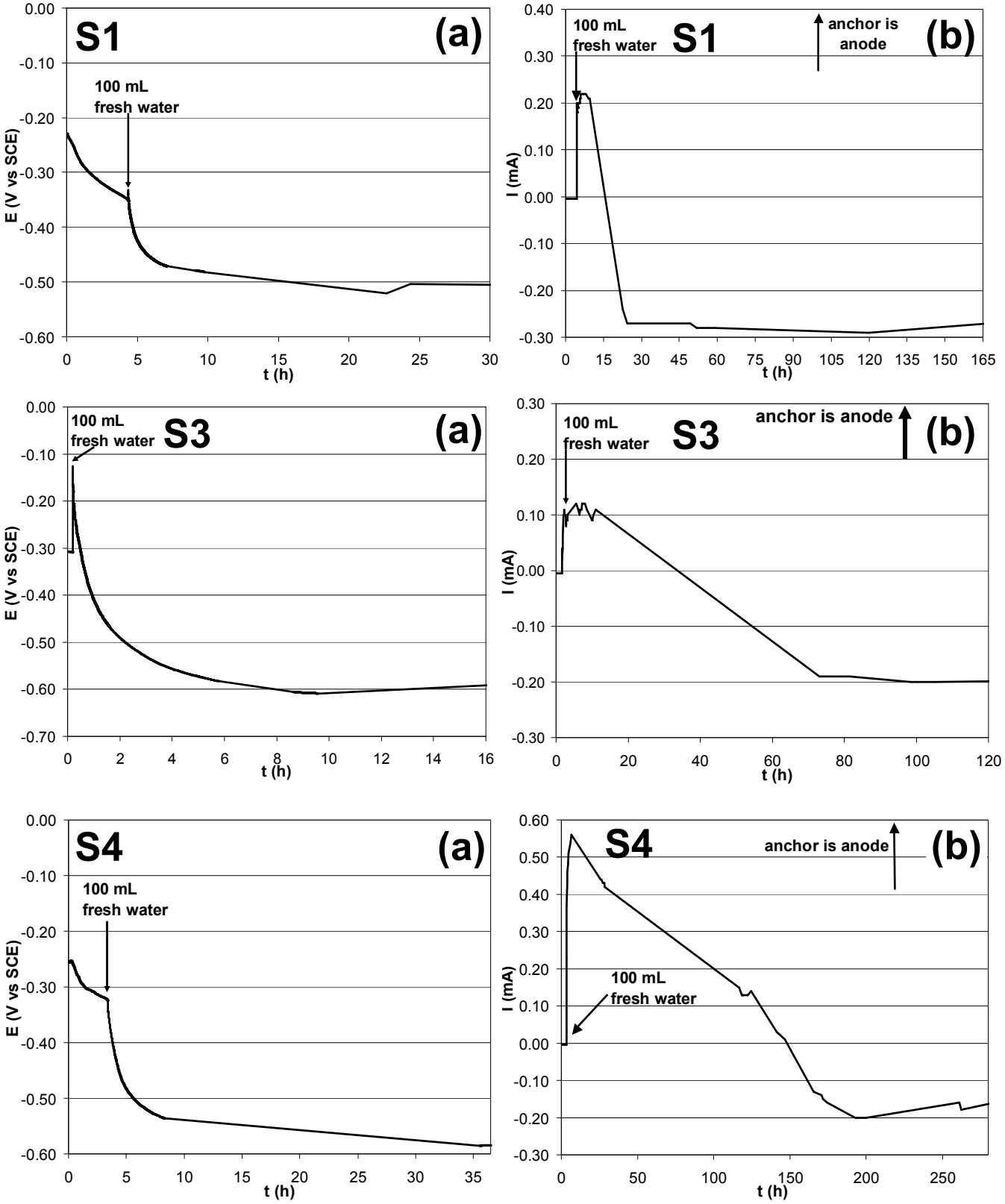

Figure 7. Potential (a) and current (b) trends of anchor-strand system for S assemblies (the arrow indicates the water addition).

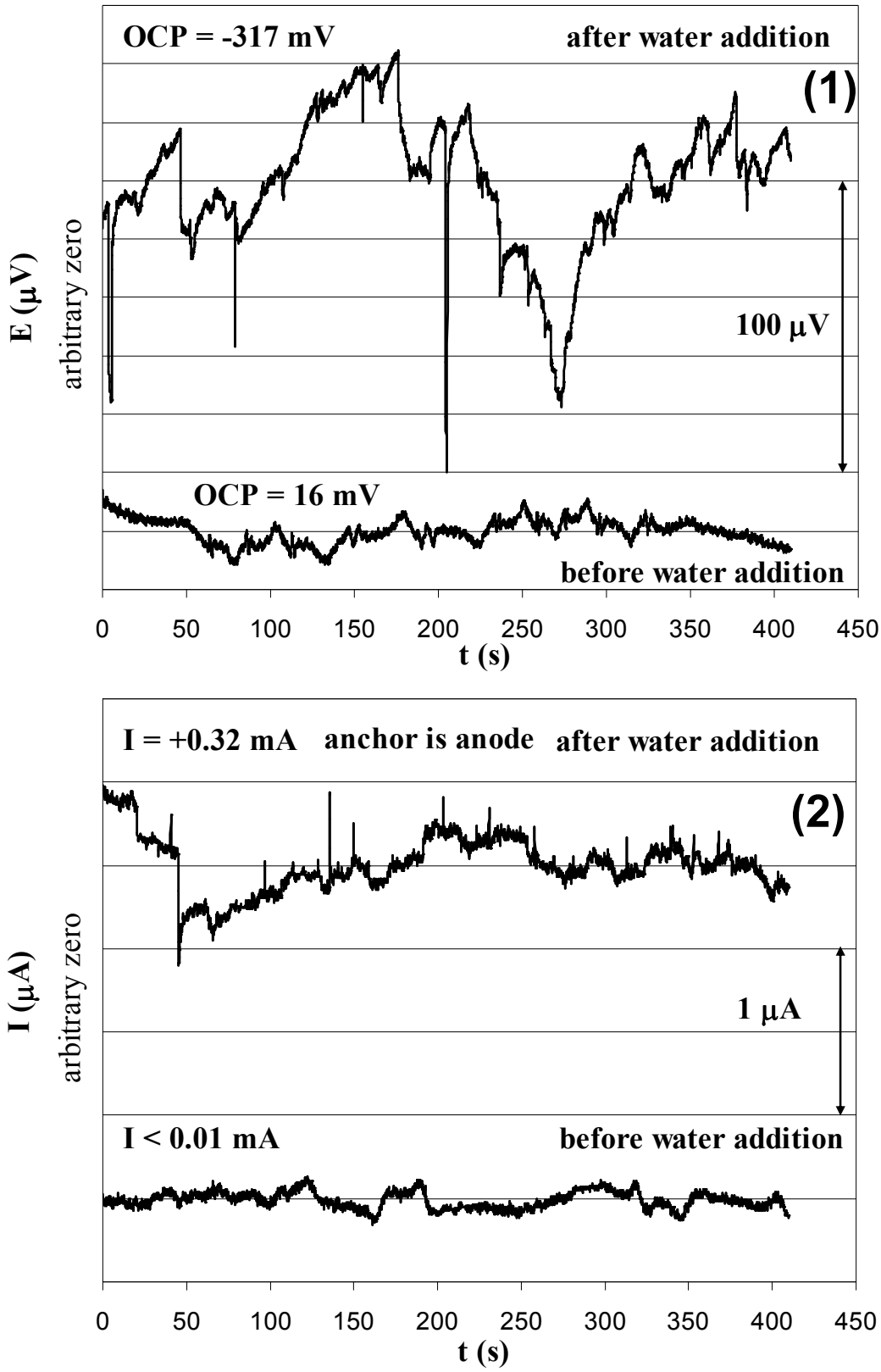

Figure 8a. OCP (1) and galvanic current (2) noise of the anchor-strand system for P1 assembly before and after fresh water addition.

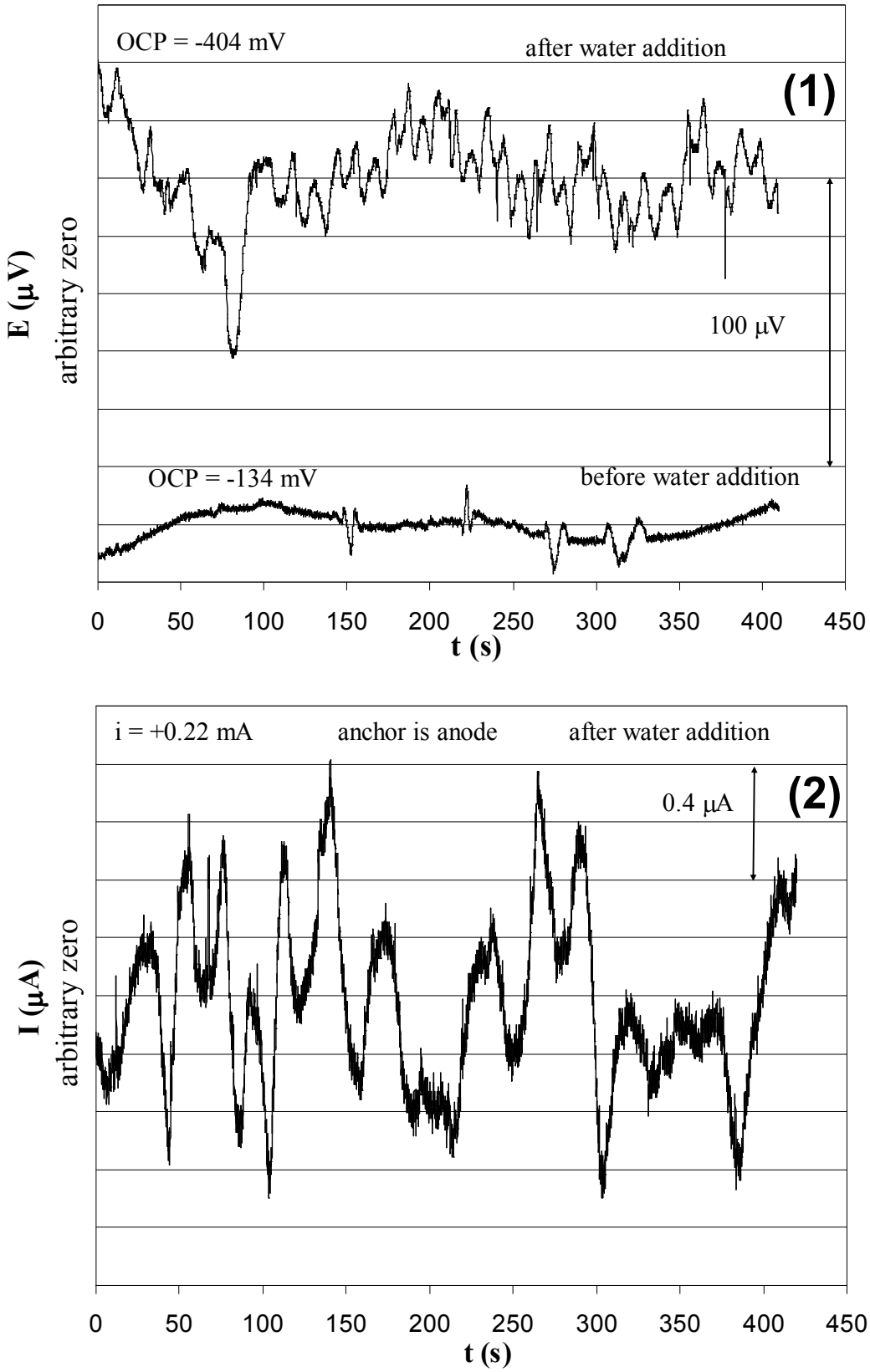

Figure 8b. OCP (1) and galvanic current (2) noise of the anchor-strand system for P2 assembly before and after fresh water addition.

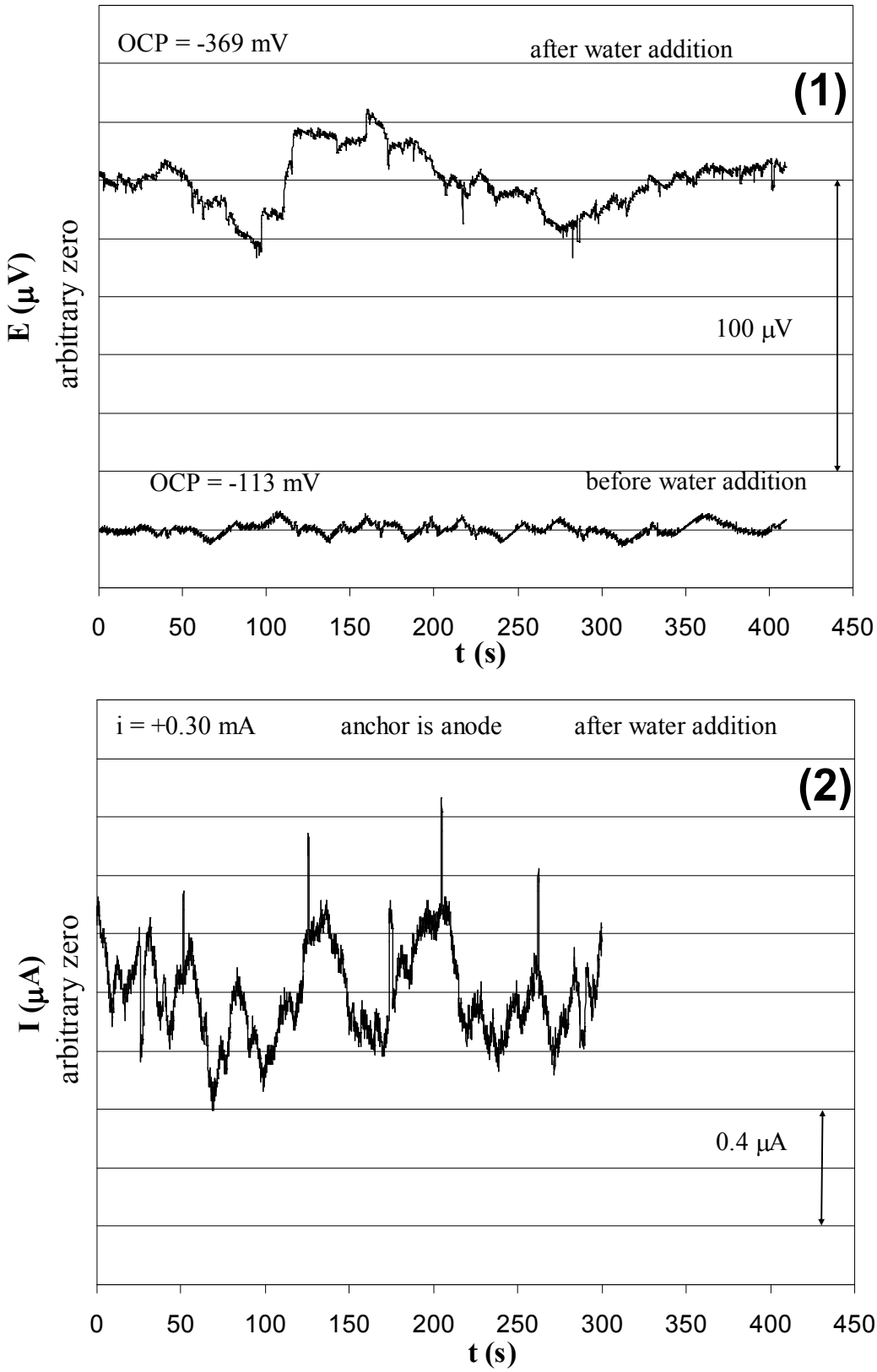

Figure 8c. OCP (1) and galvanic current (2) noise of the anchor-strand system for P3 assembly before and after fresh water addition.

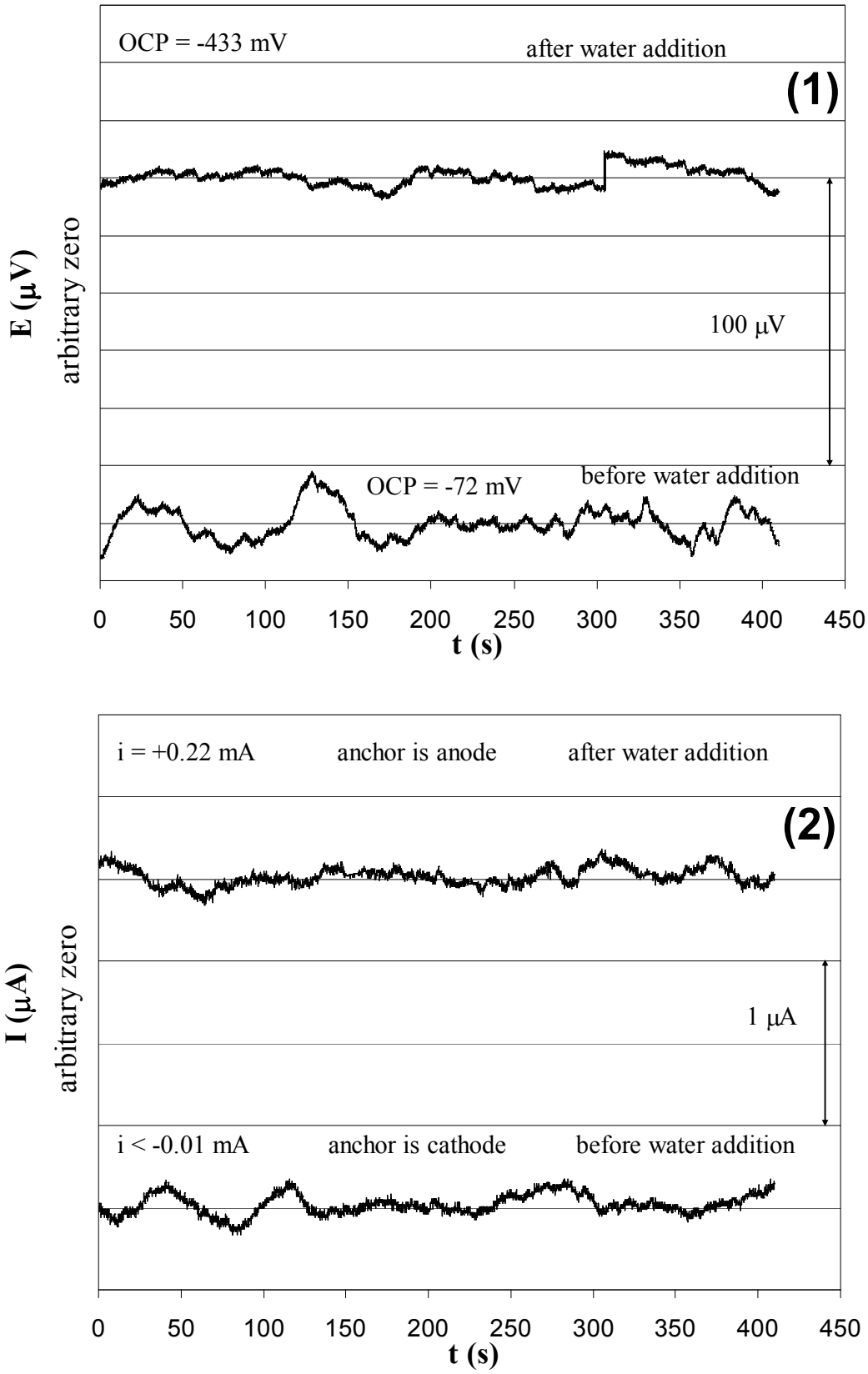

Figure 9a. OCP (1) and galvanic current (2) noise of the anchor-strand system for S1 assembly before and after fresh water addition.

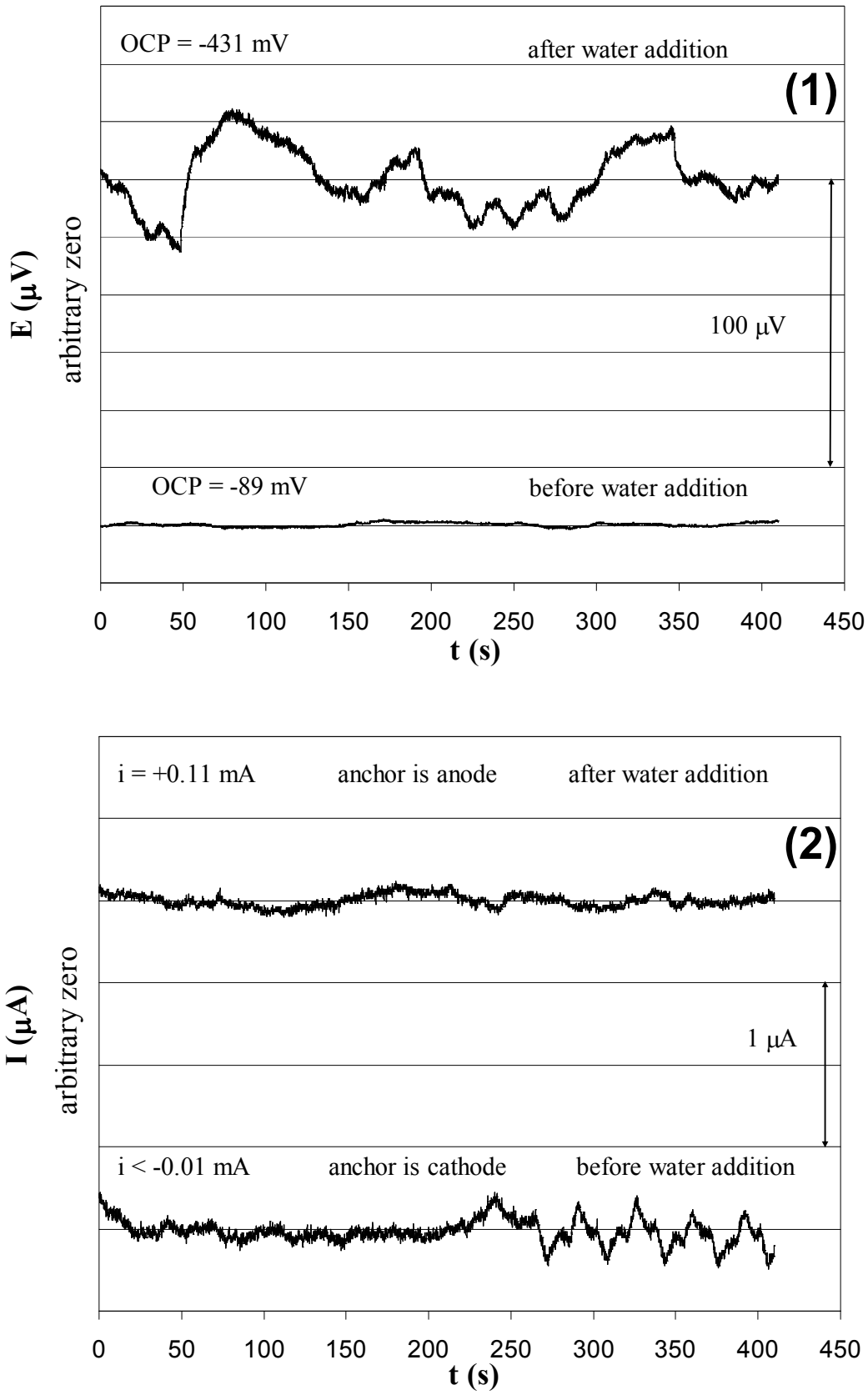

Figure 9b. OCP (1) and galvanic current (2) noise of the anchor-strand system for S3 assembly before and after fresh water addition.

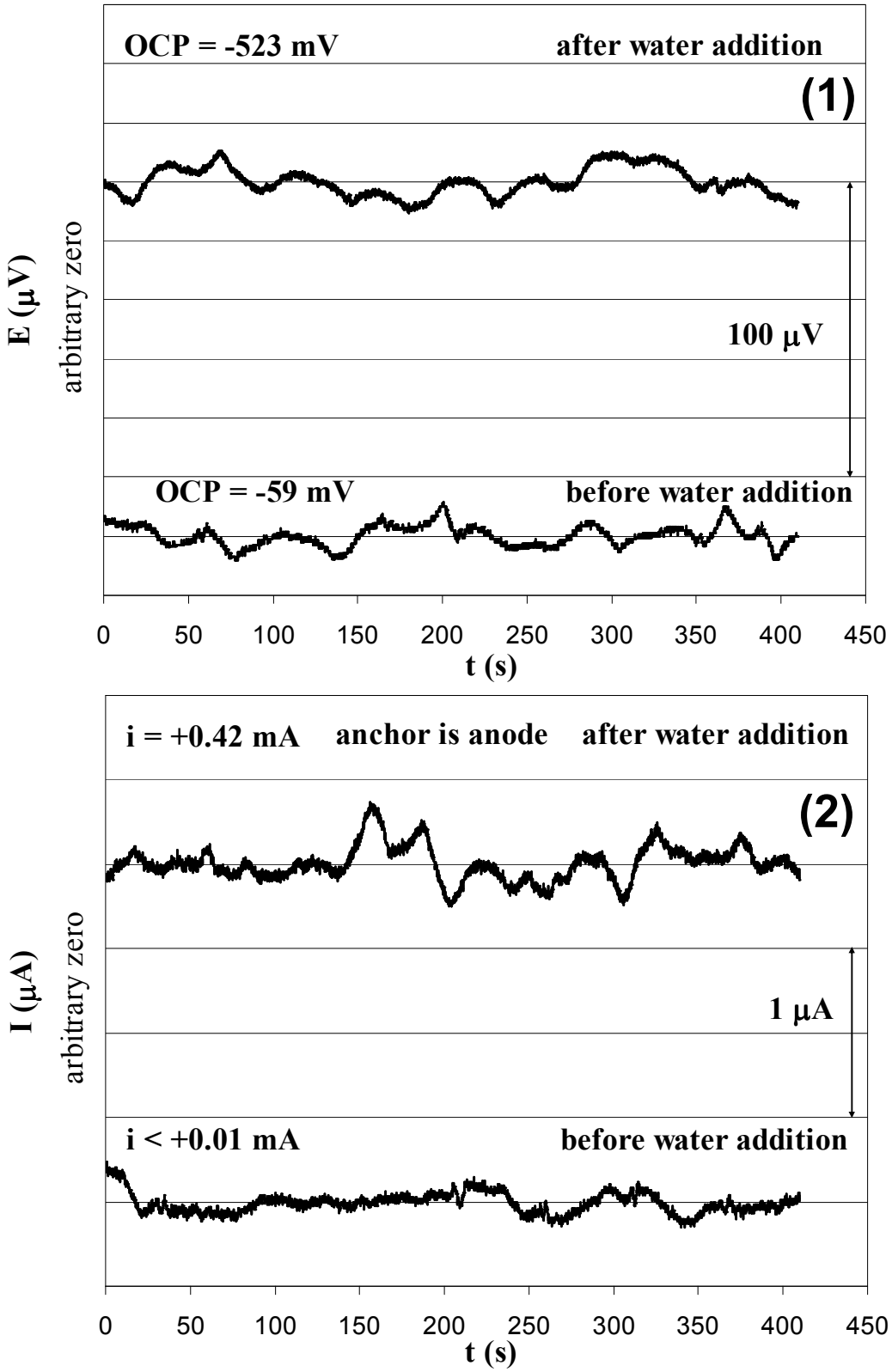

Figure 9c. OCP (1) and galvanic current (2) noise of the anchor-strand system for S4 assembly before and after fresh water addition.

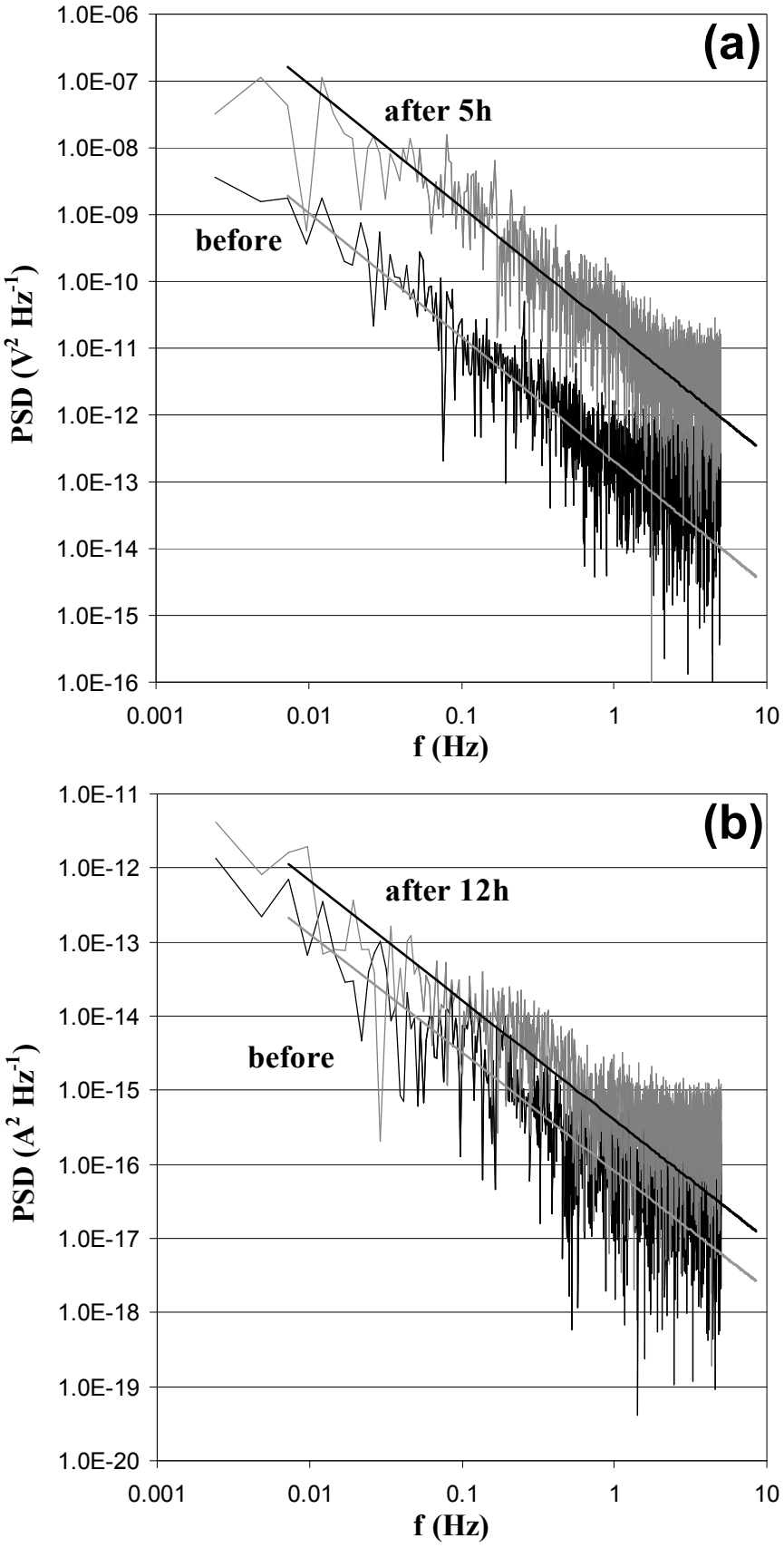

Figure 10. Potential (a) and current (b) PSD for P1 system before and after water addition.

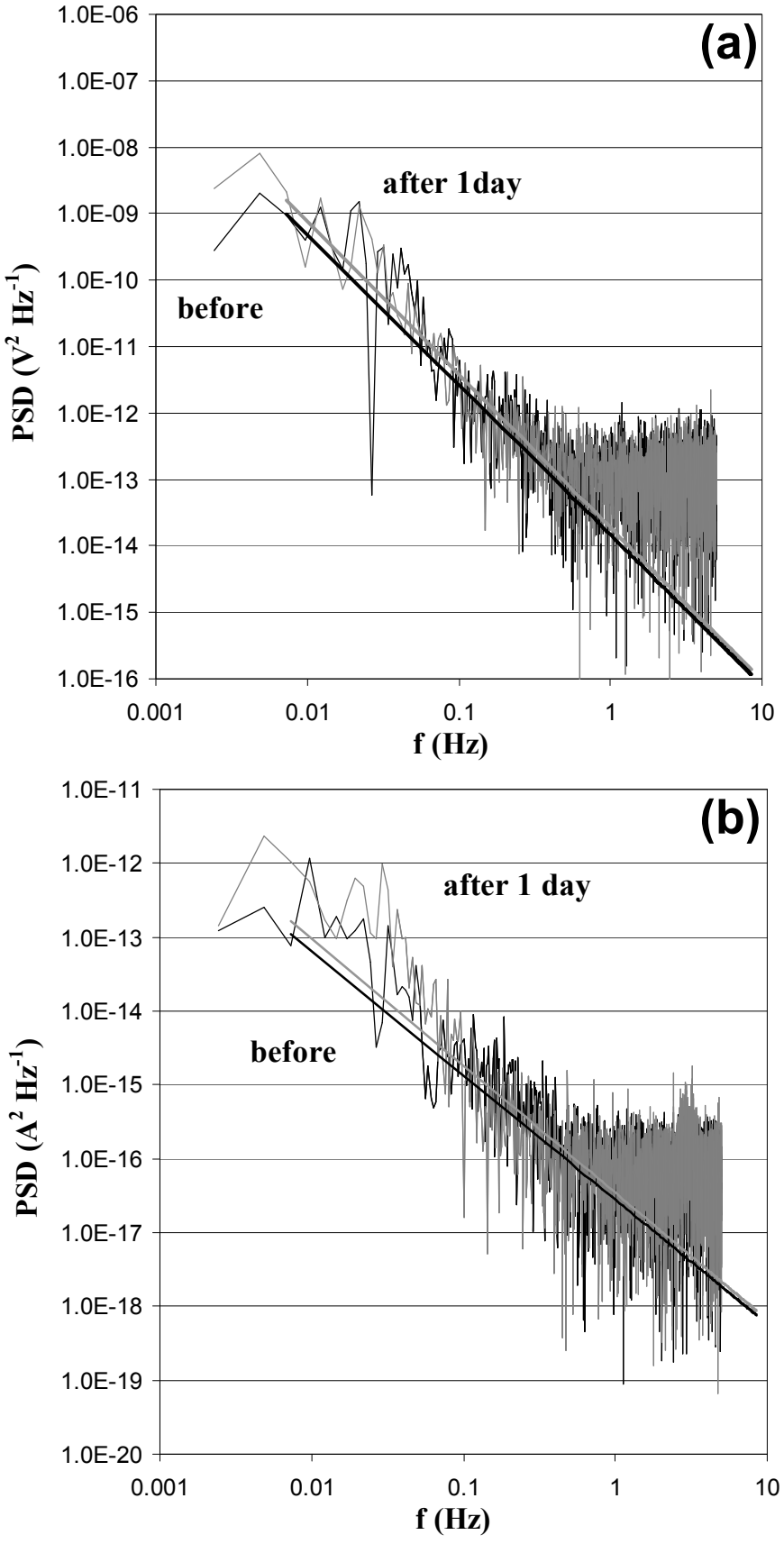

Figure 11. Potential (a) and current (b) PSD for S4 system before and after water addition.

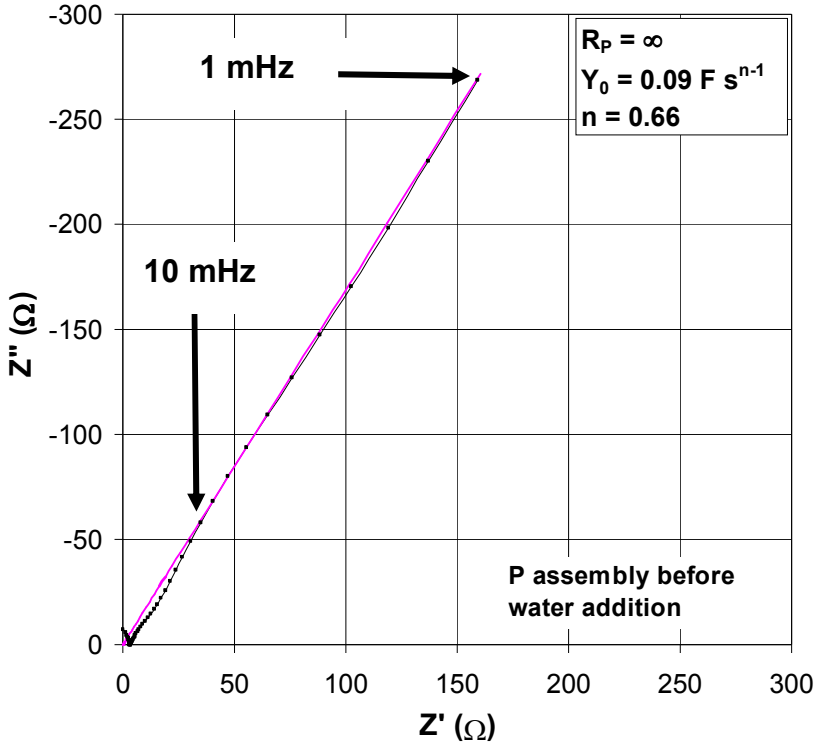

Figure 12. EIS behavior of P1 assembly before a water recharge event. The solid line indicates the low frequency model fitting as explained in text.

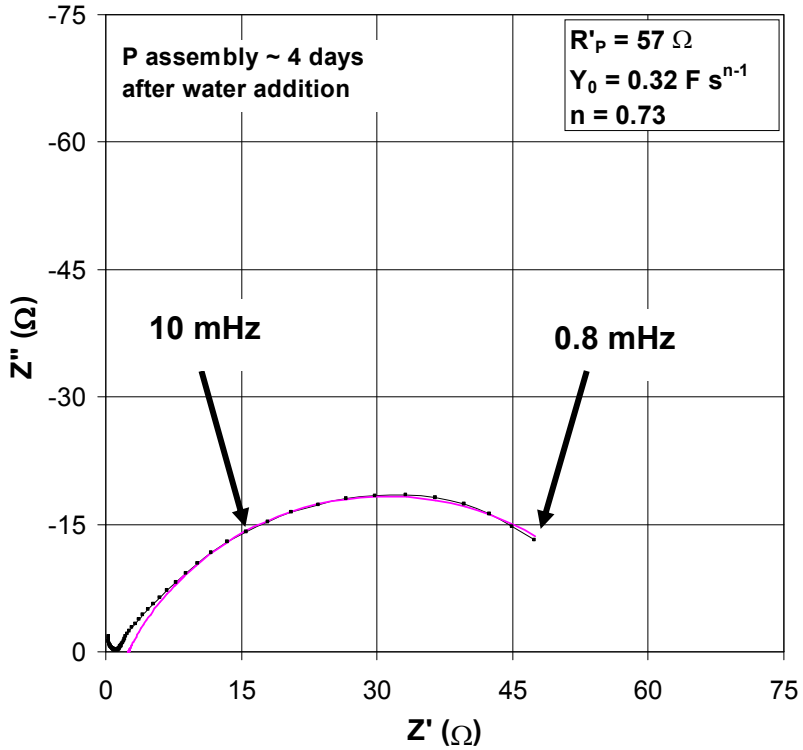

Figure 13. EIS behavior of P1 assembly after a water recharge event. The solid line indicates the low frequency model fitting as explained in text.

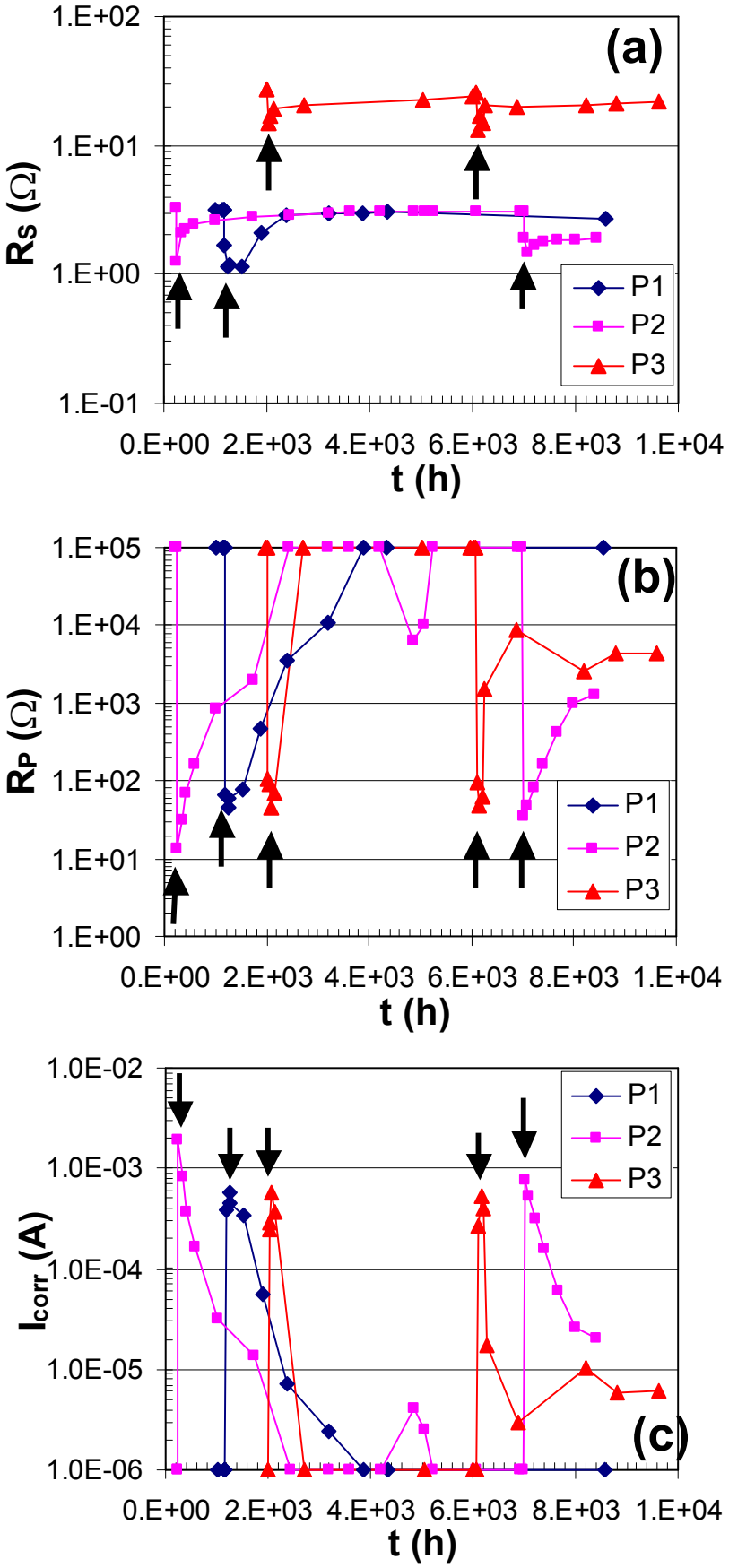

Figure 14. Electrochemical parameters, (a) R_S and (b) R_P estimated by EIS, and the corresponding (c) I_{corr} for P assemblies before and after water addition. The arrows in the diagrams indicate the water recharge events.

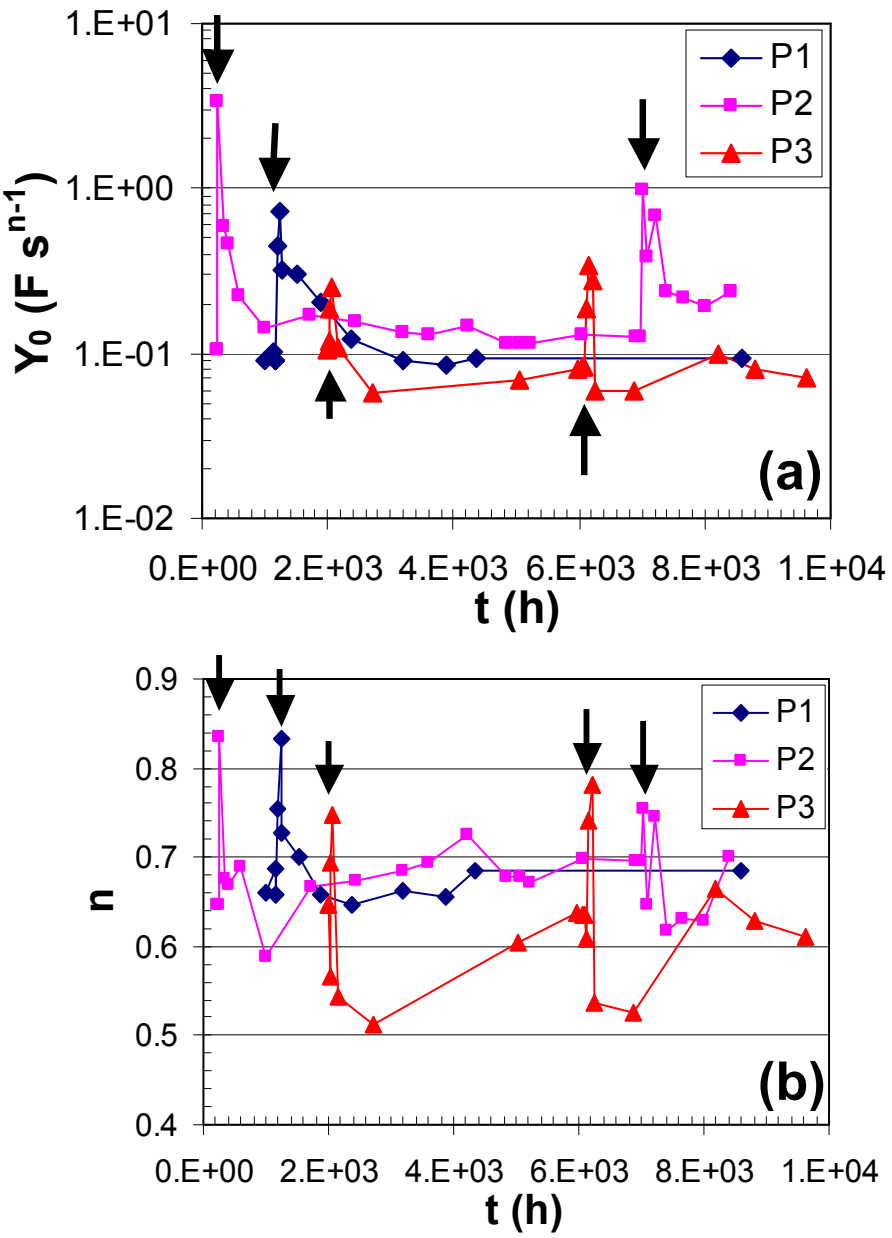

Figure 15. Electrochemical parameters, (a) Y_0 and (b) *n* estimated by EIS for P assemblies before and after water addition. Arrows indicate water recharge events.

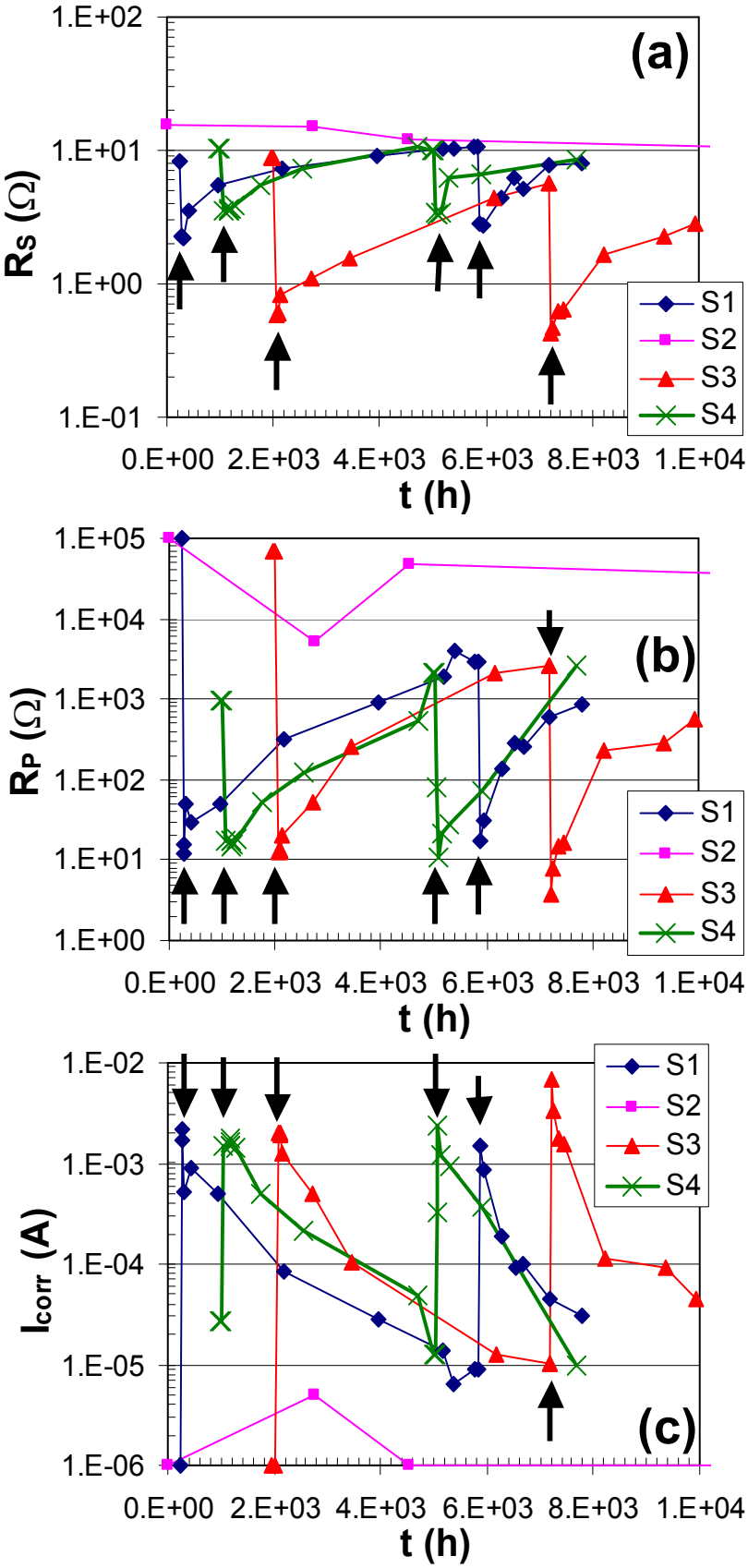

Figure 16. Electrochemical parameters, (a) R_S and (b) R_P estimated by EIS, and the corresponding (c) I_{corr} for S assemblies before and after water addition. Arrows indicate water recharge events.

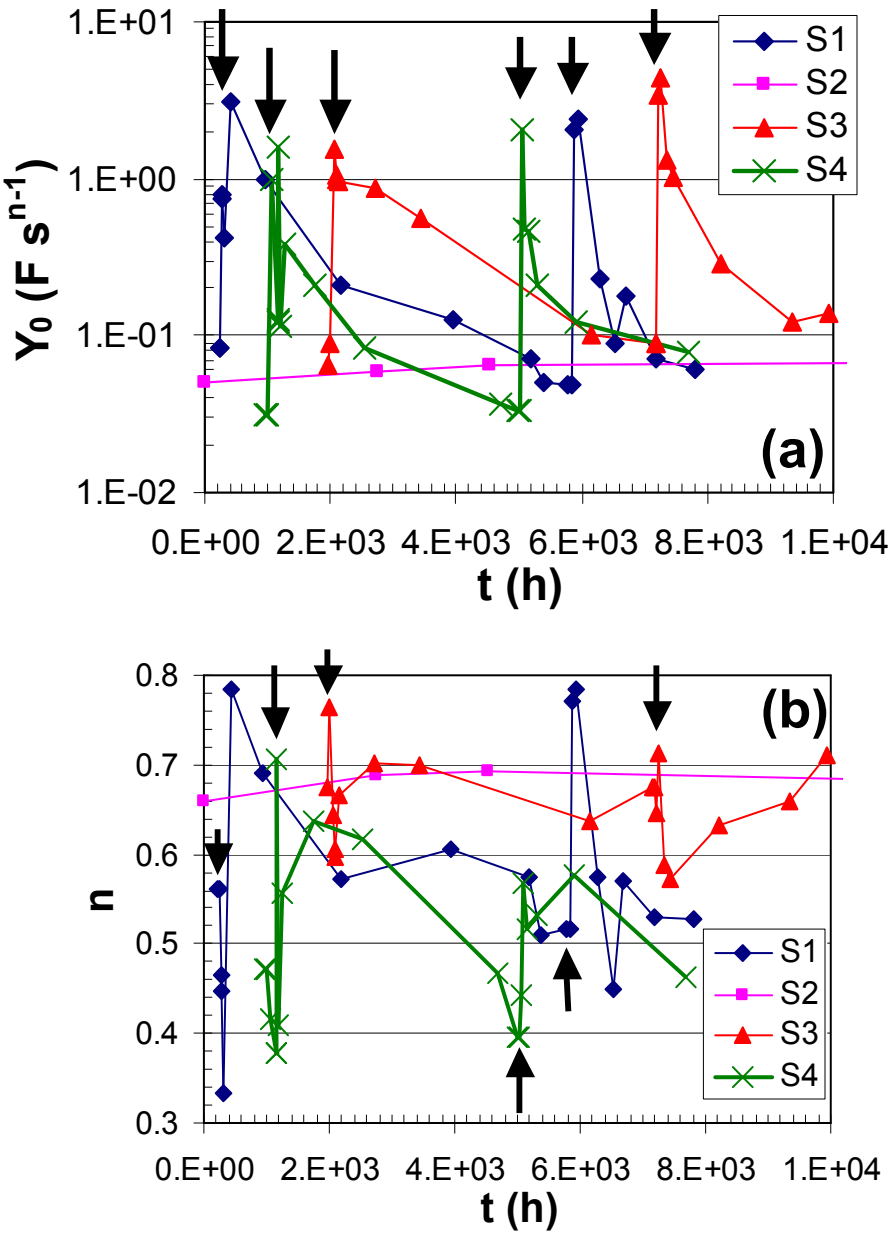

Figure 17. Electrochemical parameters, (a) Y_0 and (b) n estimated by EIS for S assemblies before and after water addition. Arrows indicate water recharge events.

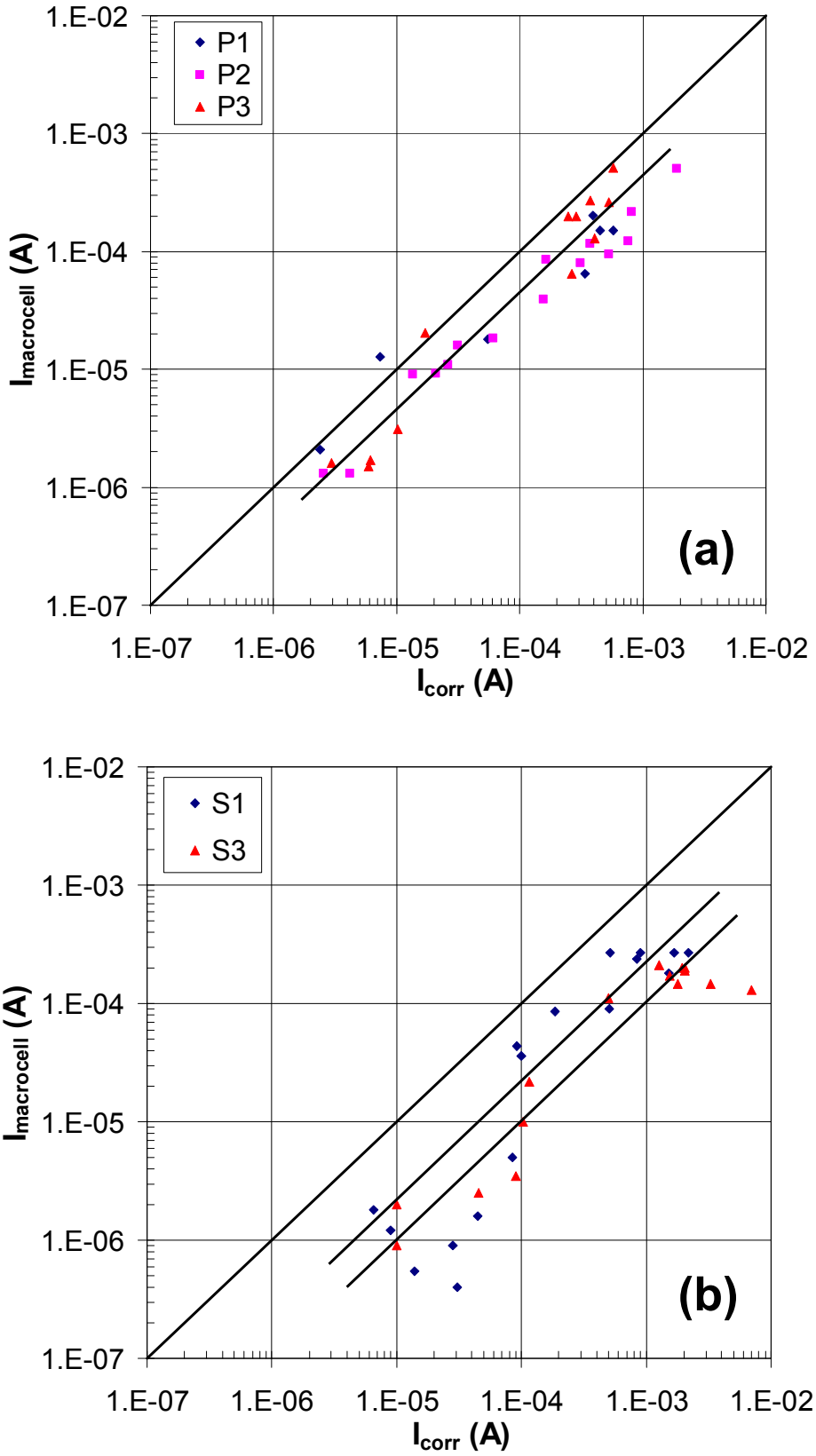

Figure 18. Comparison between $I_{macrocell}$ and the total I_{corr} estimated by EIS for (a) P and (b) S assemblies.

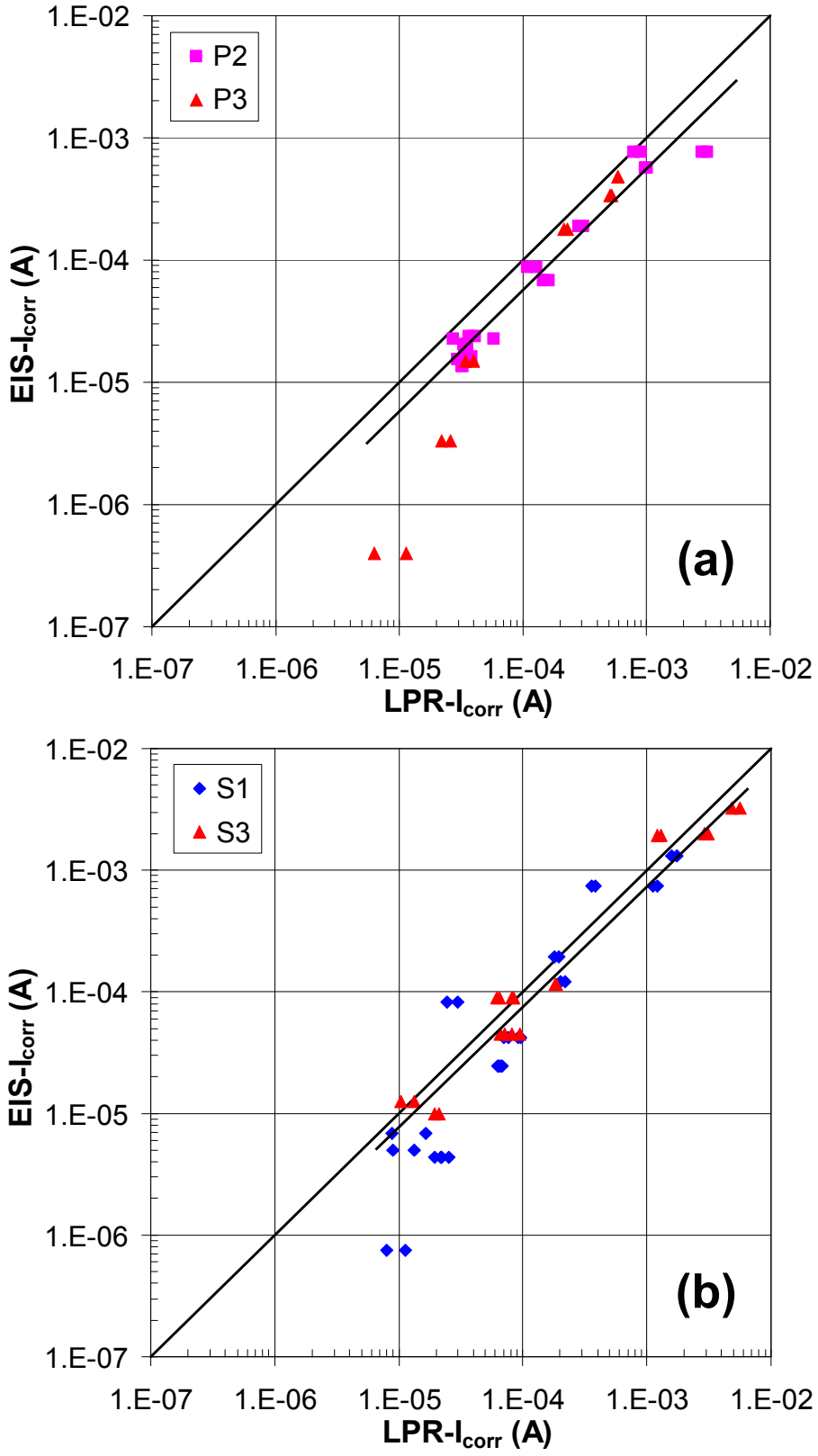

Figure 19. Comparison of total I_{corr} estimated by EIS and LPR for (a) P and (b) S assemblies.

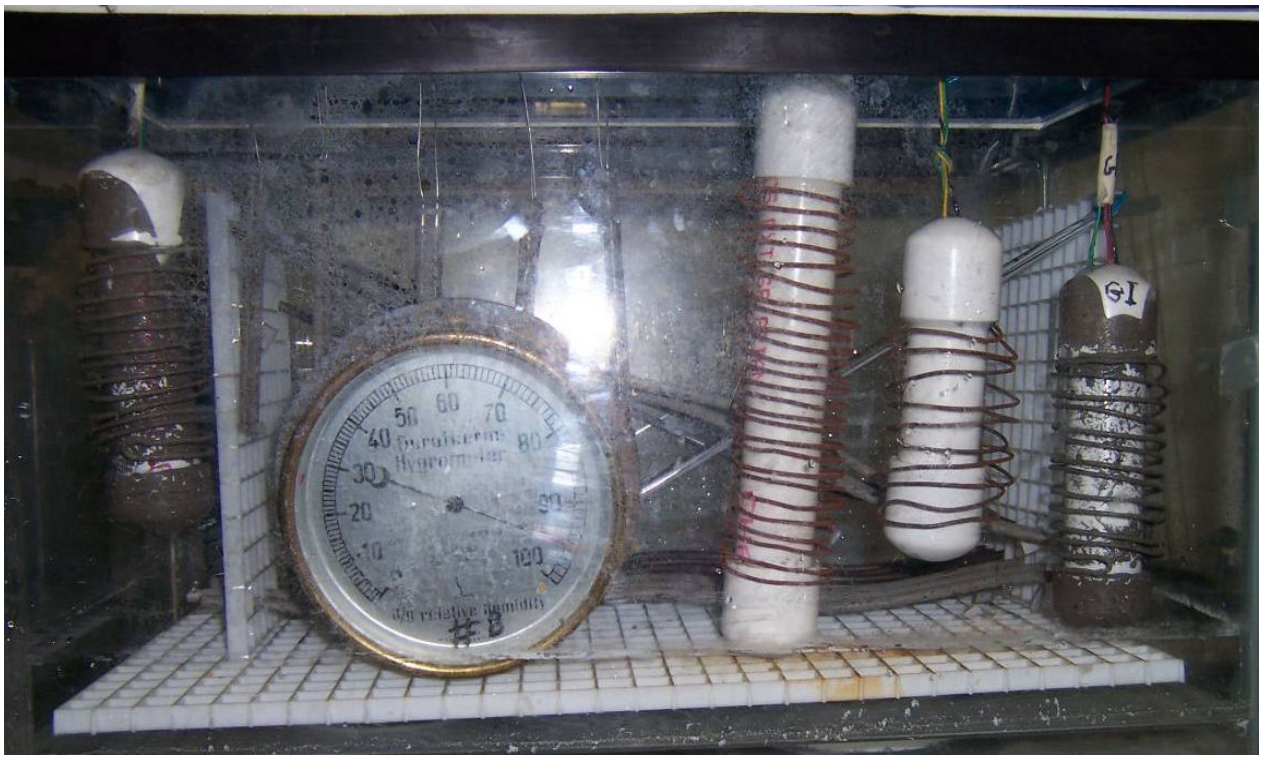

Figure 20. 95% RH chamber used in the atmospheric corrosion experiments.

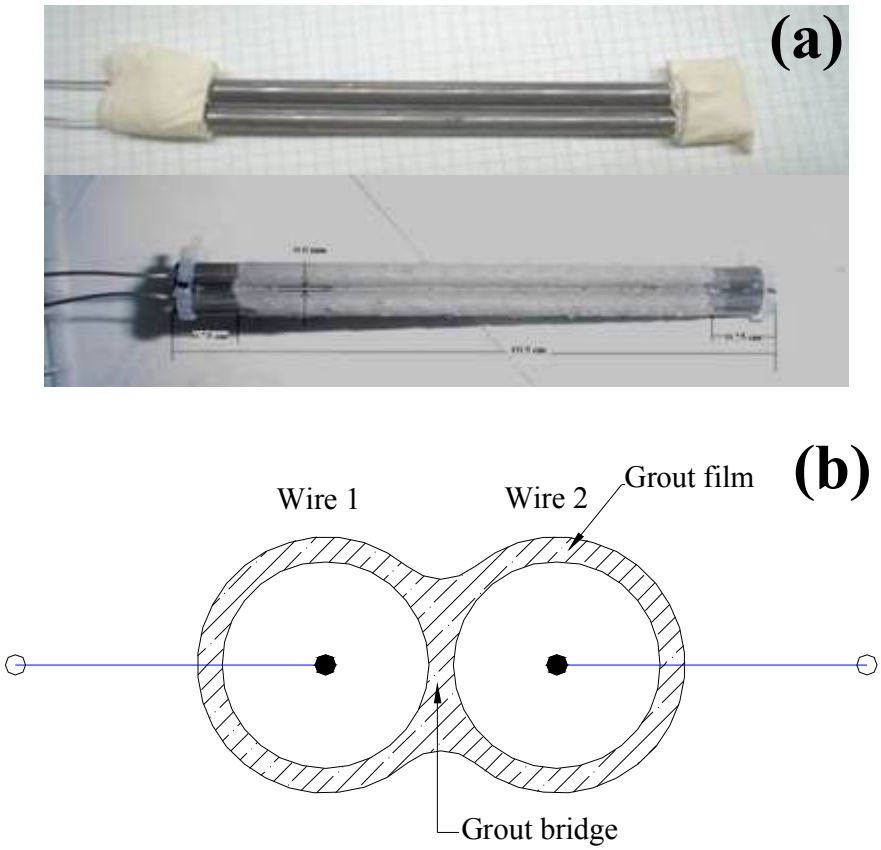

Figure 21. (a) WGW probes and (b) schematic of probe cross-section.

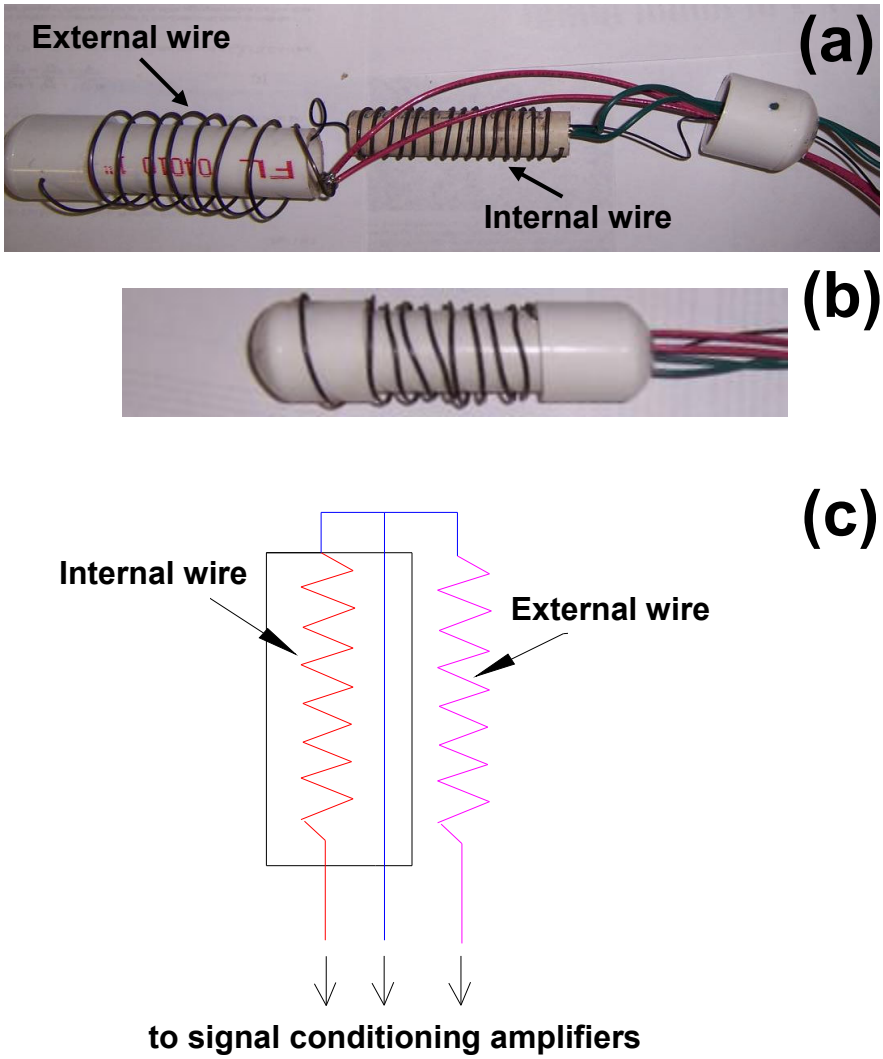

Figure 22. ER probes (a) before assembly and (b) complete and closed probe. (c) Schematic of the ER probes. Note: shown are first generation probes with single-coiled wire. Three finalized double-coiled probes are shown in Figure 20.

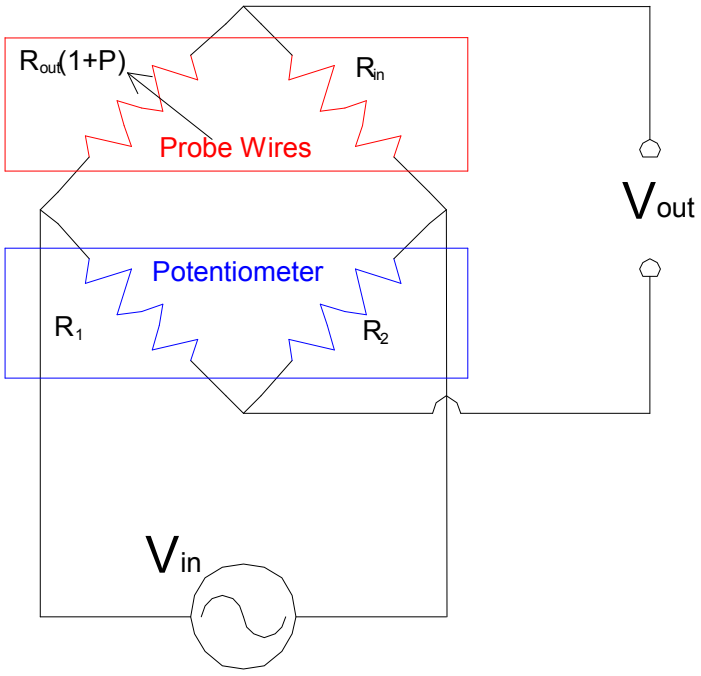

I.C.

$$@\, V_{out} = 0 \Rightarrow P = 0$$

$$\frac{R_{out}}{R_{in}} = \frac{R_1}{R_2} \approx 1$$

$$P = \frac{4 \cdot V_{out}}{V_{in} - 2 \cdot V_{out}}$$

Figure 23. Schematic of ER probe. A 0.03 μF capacitor was placed across R2 to minimize phase shift.

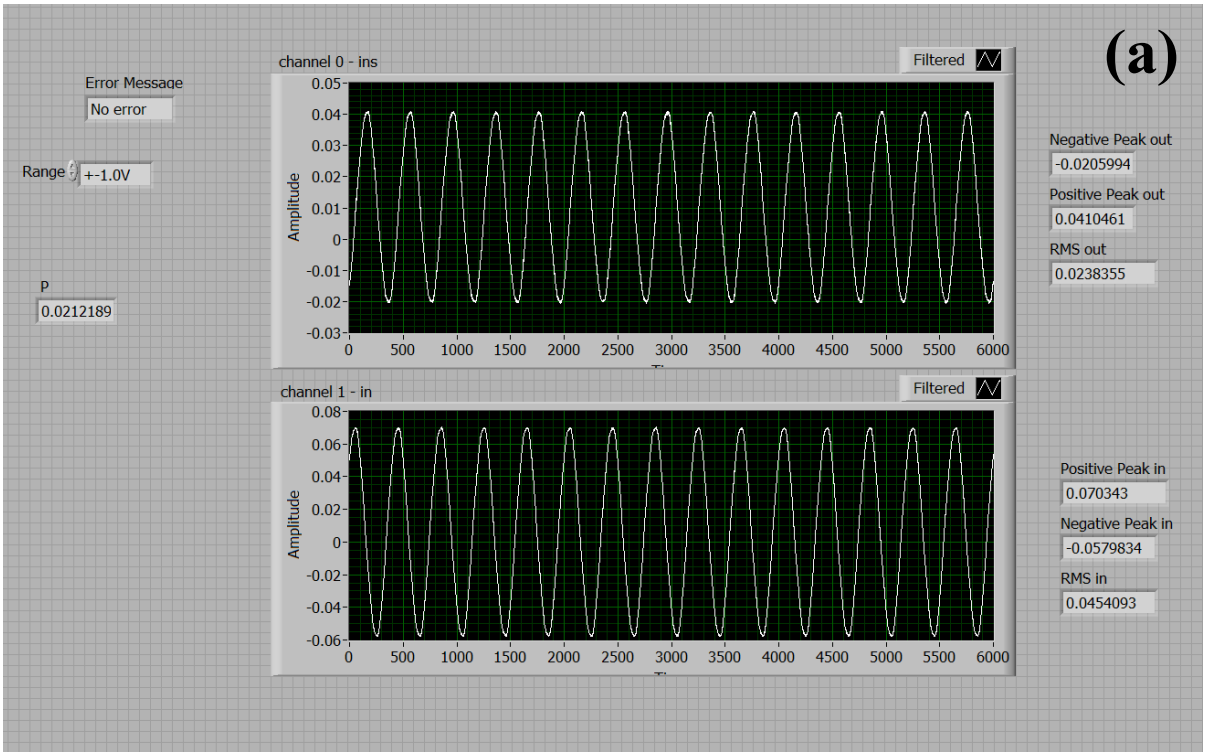

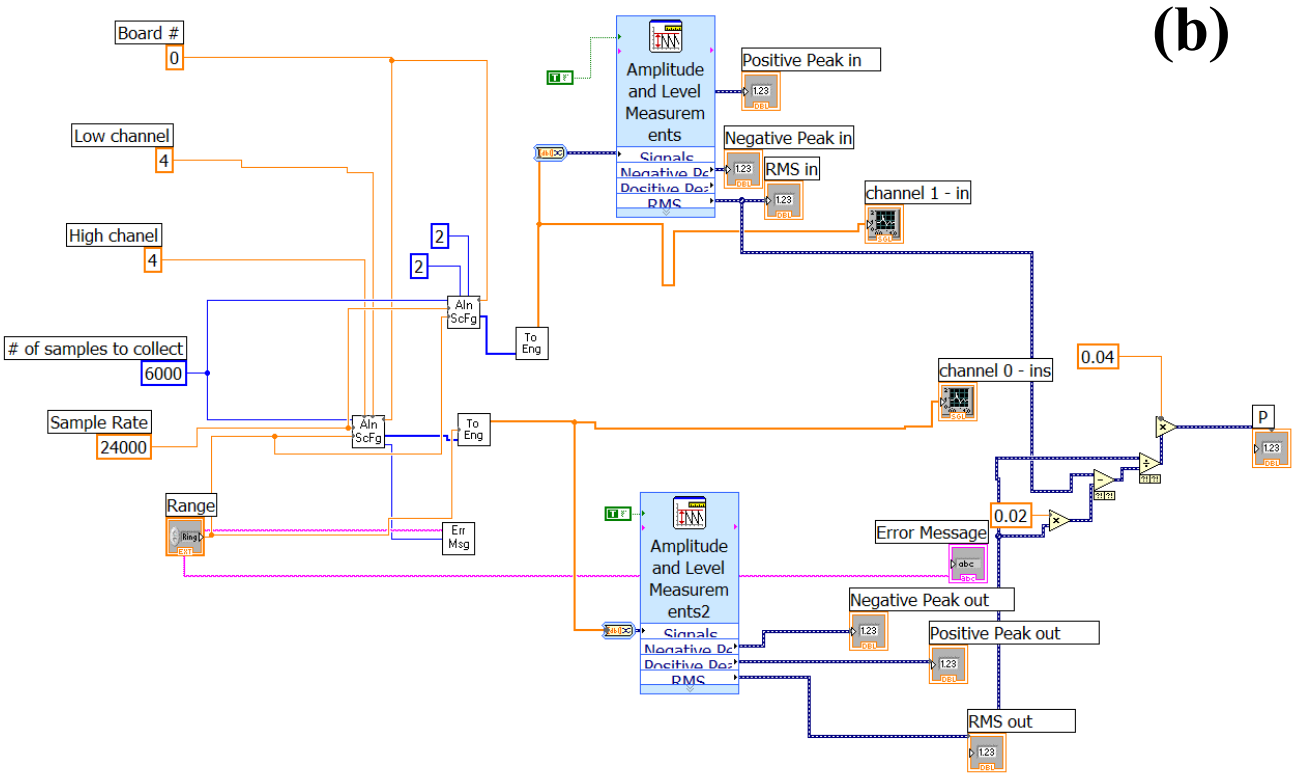

Figure 24. (a) Labview™ program developed to measure the resistance by the ER methods and (b) the corresponding block diagram.

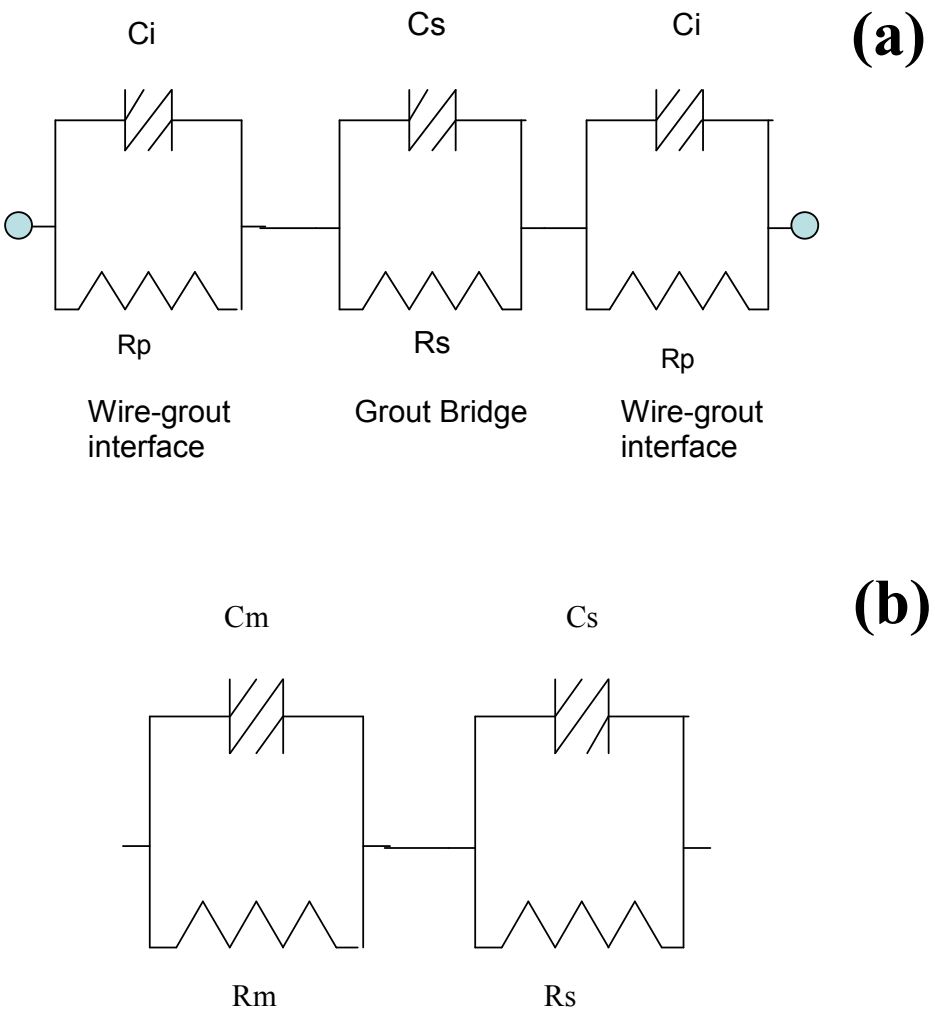

Figure 25. (a) Equivalent circuit for the electrochemical probe and (b) simplified circuit used to fit the experimental data.

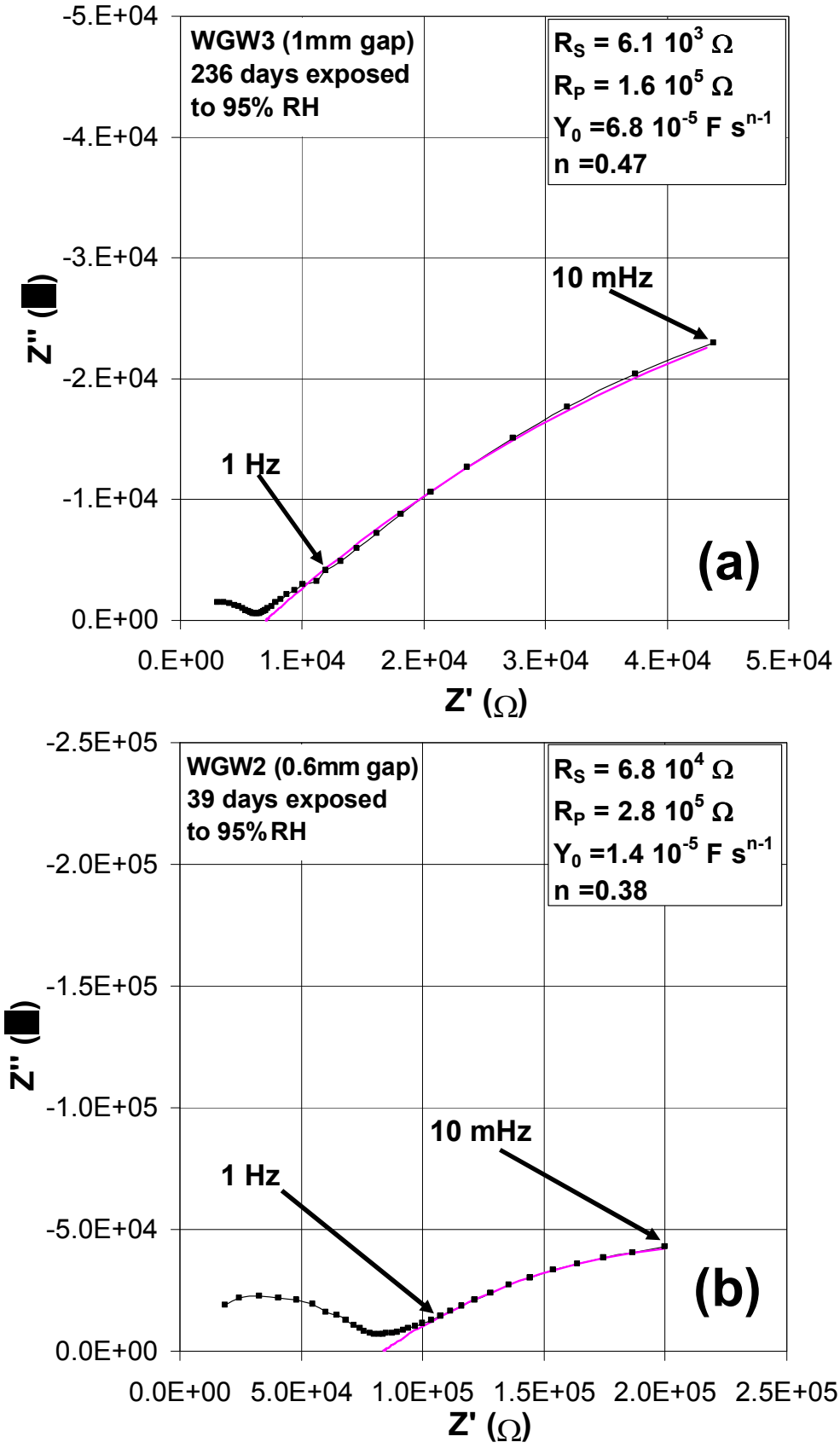

Figure 26. EIS behavior of (a) 1 mm gap and (b) 0.6 mm gap WGW probes exposed to 95% RH. The solid line indicates the low frequency model fitting as explained in text.

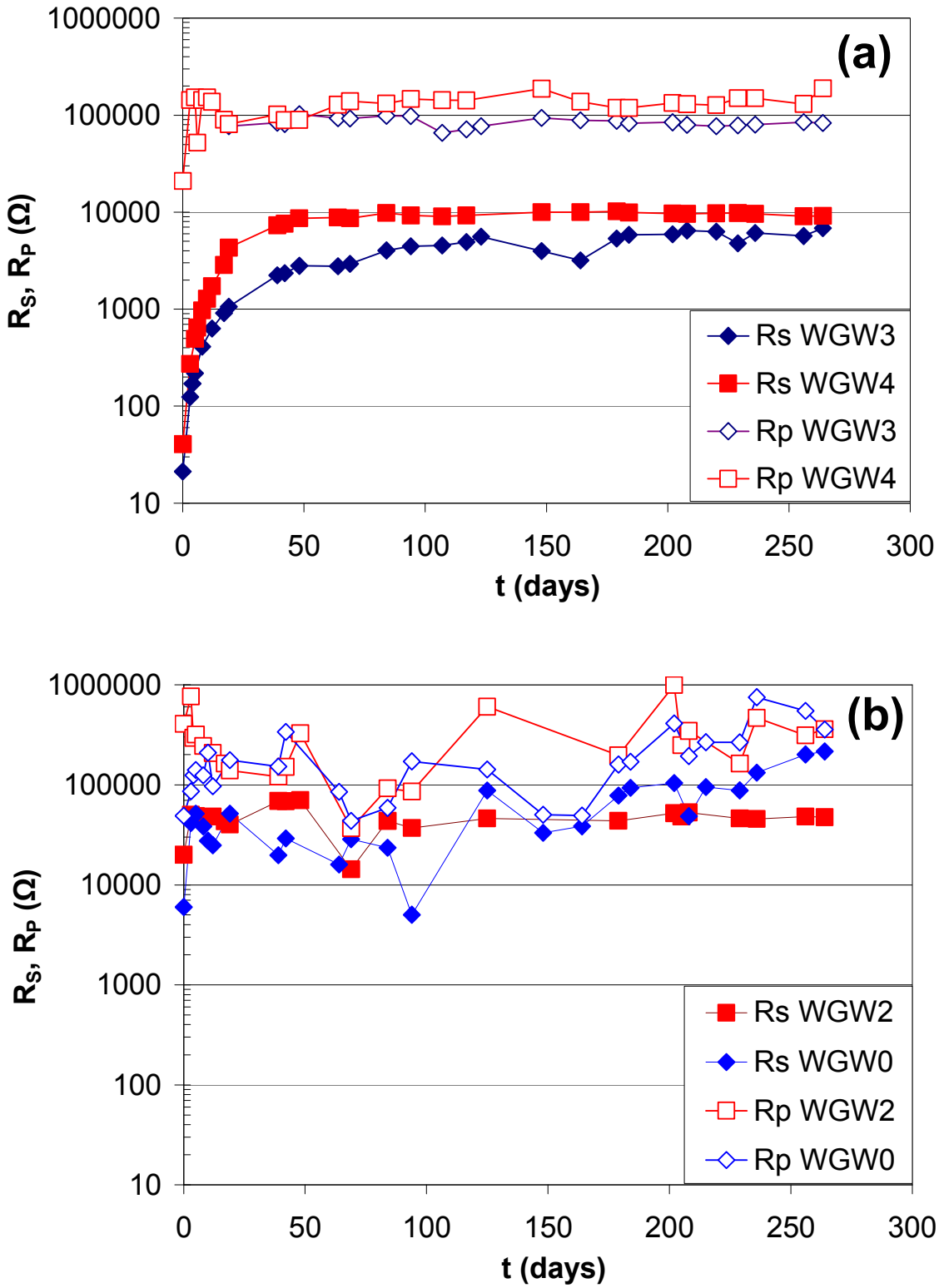

Figure 27. R_S and R_P trends for (a) 1 mm and (b) 0.6 mm gap WGW probes exposed to a 95% RH, simulating conditions in an air void around a water recharge event.

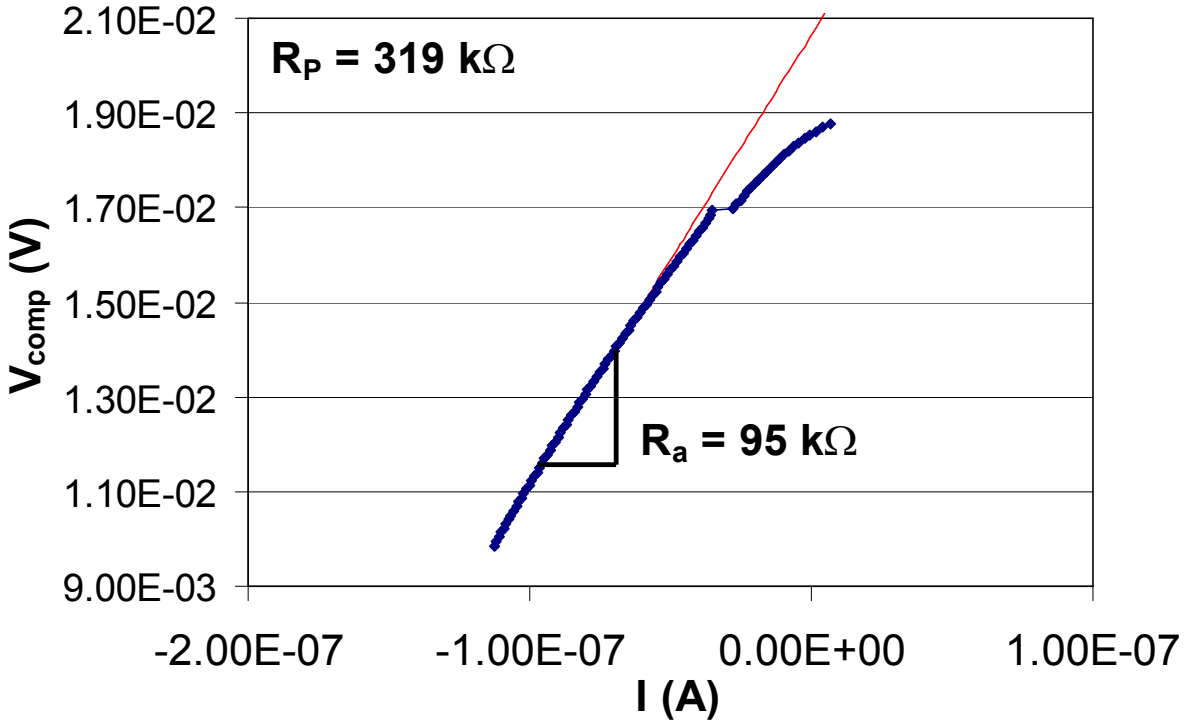

Figure 28. I-V_{comp} curve of 1 mm gap WGW probe exposed to 95% RH for 256 days, showing R_a and the R_P calculated per Eq. [7].

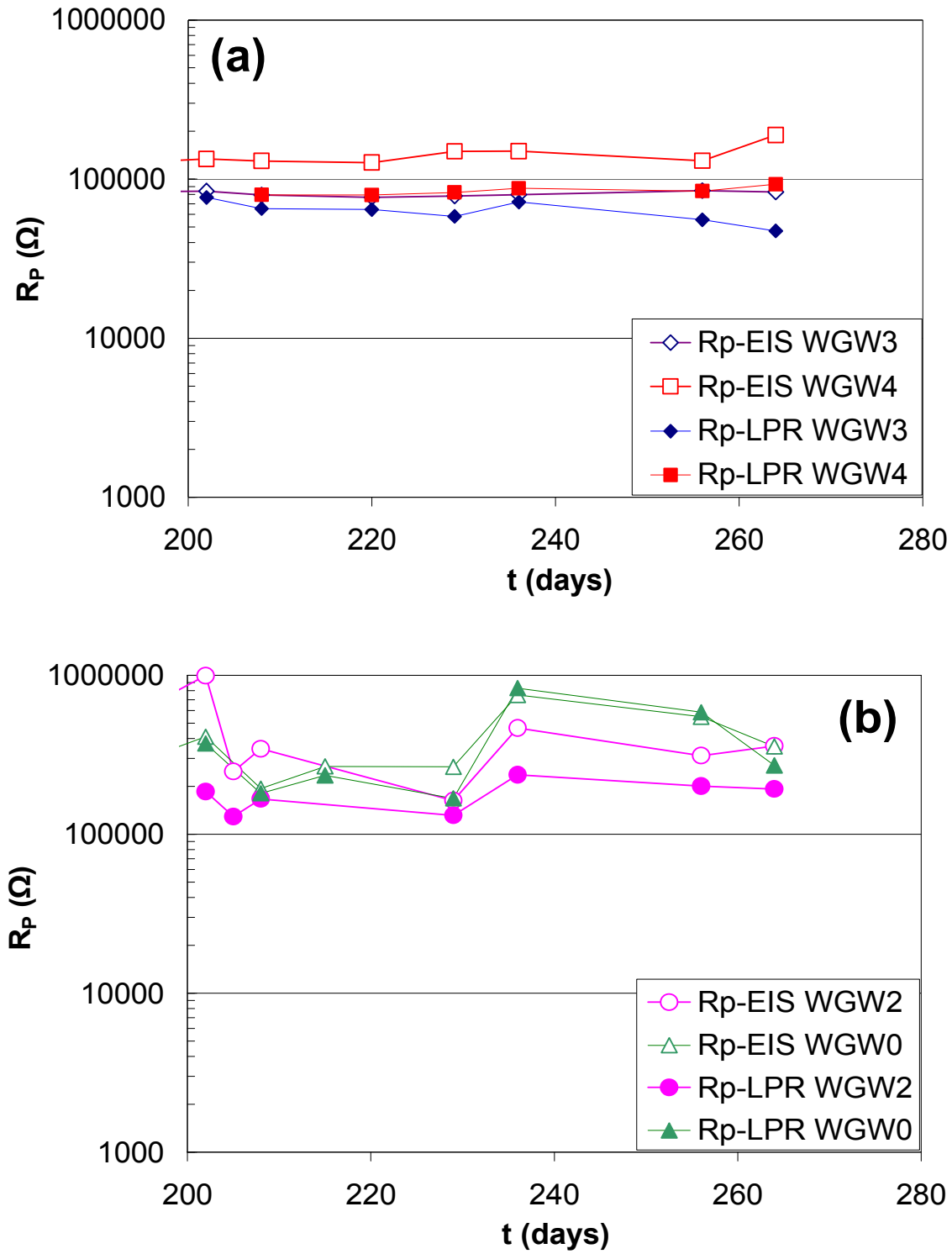

Figure 29. R_P values estimated by LPR and EIS methods for probes with (a) 1.0mm gap and (b) 0.6mm gap in a 95% RH simulated air void environment.

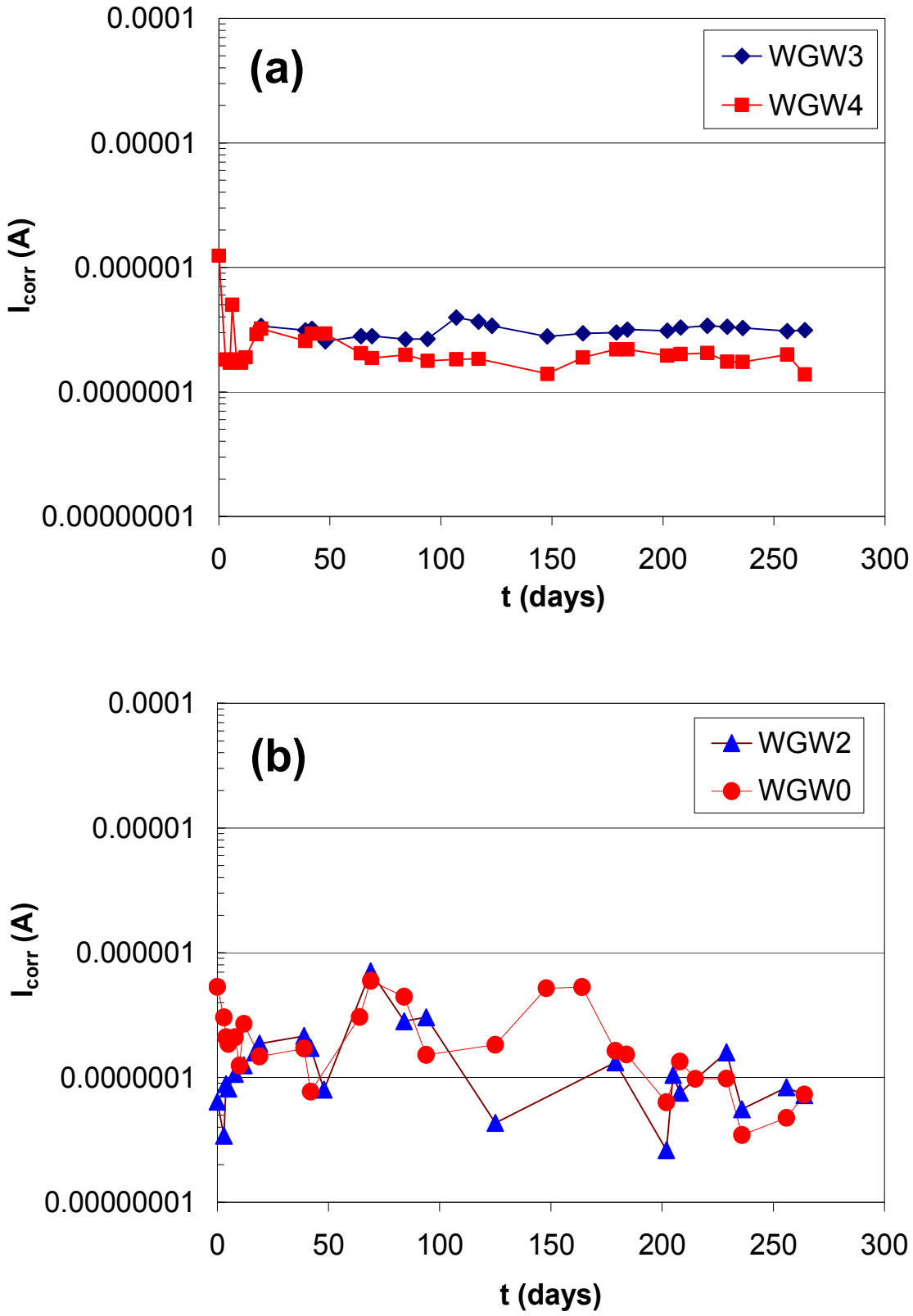

Figure 30. I_{corr} trends of WGW probes with (a) 1.0 mm and (b) 0.6 mm gap exposed to a 95% RH.

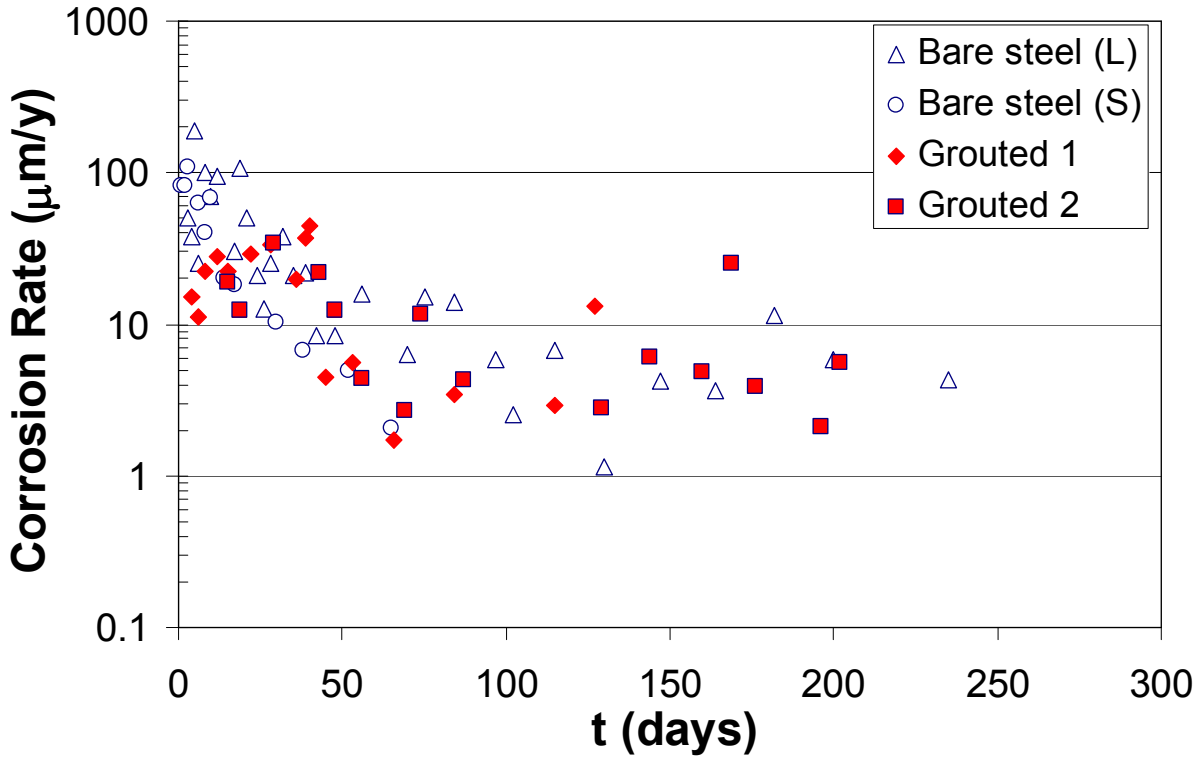

Figure 31. The instantaneous corrosion rate trends of bare and grouted ER probes exposed to a 95% RH.

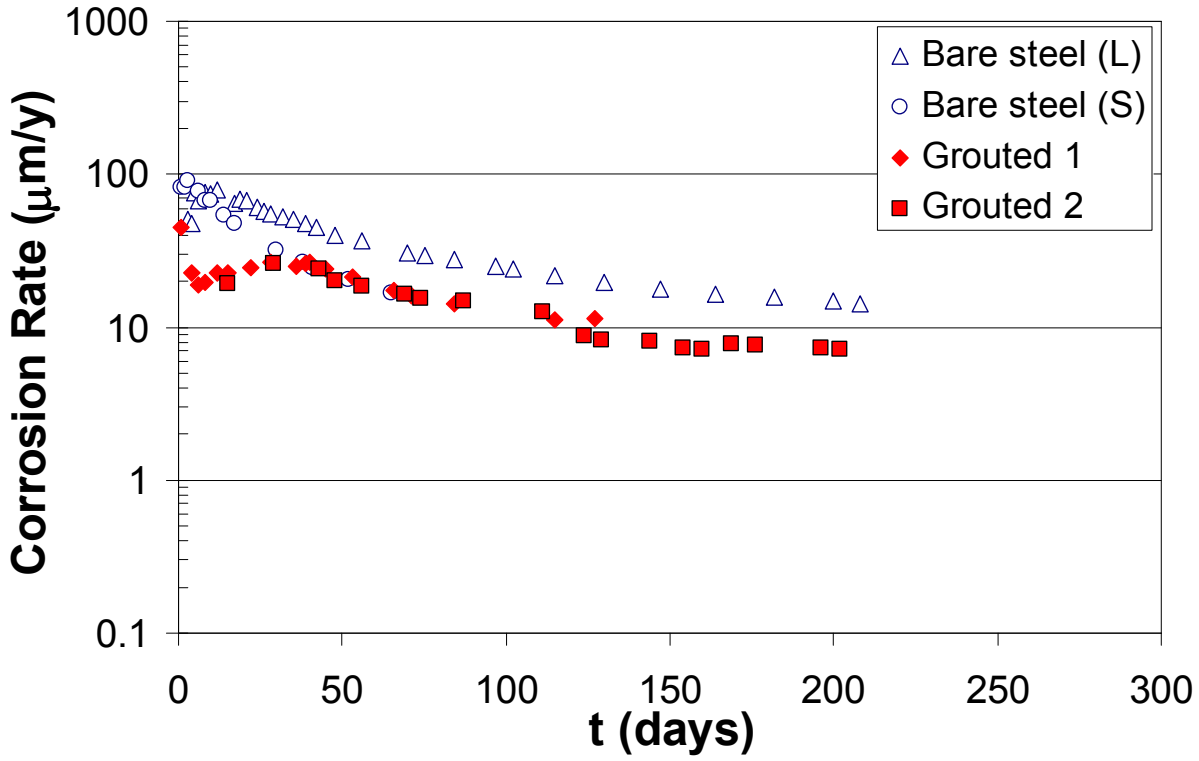

Figure 32. Cumulative corrosion rate trends of grouted and bare ER probes exposed to a 95% RH.

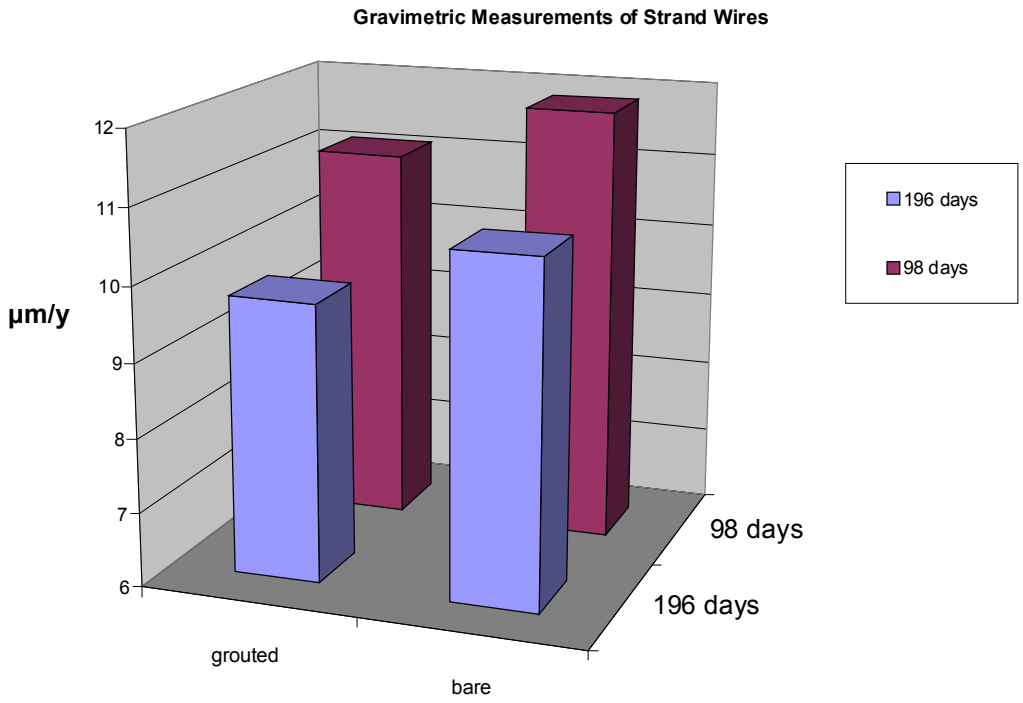

Figure 33. Corrosion rate of grouted and bare steel strands exposed to a 95% RH, estimated by weight loss measurement.